Spring 2022

Dissecting the Contributions of Langerhans Cells to Skin Wound Healing and the Angiogenic Niche

Renee R. Wasko
Yale University Graduate School of Arts and Sciences, renee.wasko@yale.edu

Abstract

Dissecting the Contributions of Langerhans Cells to Skin Wound Healing and the Angiogenic Niche

Renee Rhodes Wasko

2022

Mammalian skin is complex, heterogeneous, and essential for survival. It is the primary barrier that protects us from physical, microbial, and chemical hazards, and must therefore be highly regenerative. When skin is wounded, healing occurs through a series of temporally-overlapping and tightly regulated stages of inflammation, proliferation, and remodeling. Angiogenesis, the growth of new blood vessels from pre-existing vessels, occurs during the proliferative phase of repair and is essential for the formation of new, healthy tissue. Blood vessels are a vital source of oxygen, nutrients, and immune cells, and failure of these vessels to regenerate after injury results in chronic, non-healing wounds. Chronic wounds represent a staggering portion of global healthcare costs, and these costs will continue to rise as the population grows older and more diabetic. It is therefore imperative that we thoroughly characterize the signals that govern angiogenesis in order to inform the development of new, effective therapies to rescue skin revascularization and healing.

The two major goals of this work are (I) to characterize the angiogenic niche in healing skin, and (II) to determine if Langerhans cells (LCs), a type of phagocytic, skin-resident immune cell, play a role in skin revascularization and repair. We provide a map of an early angiogenic niche by analyzing single-cell RNA sequencing of mouse skin wound healing. Within skin wounds, endothelial cells receive several, specialized signals from multiple cell types, including well-described interactions with fibroblasts, macrophages, and keratinocytes. These data also implicate LCs in driving angiogenesis during skin repair. Using lineage-driven reporters, three-dimensional (3D) confocal microscopy, and mouse genetics, we show that LCs are spatially situated at the leading vascular edge of skin wounds and are necessary for angiogenesis during wound repair. These data provide future avenues for the control of angiogenesis to treat disease and chronic wounds, and extend the function of LCs beyond their canonical role in antigen presentation and T-cell immunity.

Dissecting the Contributions of Langerhans Cells to Skin Wound Healing and the Angiogenic Niche

A Dissertation
Presented to the Faculty of the Graduate School
Of
Yale University
In Candidacy for the Degree of
Doctor of Philosophy

By
Renee Rhodes Wasko

Dissertation Director: Valerie Horsley, Ph.D.

May 2022

Acknowledgments

This work was made possible by the hard work, creative thinking, expertise, and incredible support of so many colleagues, family members, and friends.

I want to first thank my PhD adviser, Valerie Horsley, for showing me what it is to do creative, impactful, and collaborative science. From my first week rotating in the lab, I was inspired by Valerie's process of identifying important, unanswered biological questions, and then assembling the best tools and team to answer those questions. As a trainee in Valerie's lab, I had the opportunity to "grow up" feeling supported to pursue the best and most important experiments, and to ask for help early and often. Valerie's insights on my project were invaluable. I came away from virtually every meeting with fresh perspective, ideas, and inspiration about my project, which ultimately resulted in our novel characterization of angiogenesis in skin cell types beyond Langerhans cells that I hope will prove helpful for our lab and many others.

My training also benefitted greatly from the input of my thesis committee: Drs. Kathryn Miller-Jensen, Josien van Wolfswinkel, Carla Rothlin. Each of my committee meetings was a source of new ideas, helpful input, thoughtful questions, and meaningful support. It was especially inspiring to be advised and challenged by a team of exceedingly bright, accomplished, and creative female scientists. Additionally, I want to thank Dr. John Carlson for agreeing to serve as a reader for my thesis less than a month before its submission. I am enormously grateful for John's time and willingness to evaluate this work, particularly on such short notice.

A transformational junction in my research was the shift to exploring the transcriptional regulators of skin angiogenesis more broadly, and I am extremely grateful to Dr. Kathryn Miller-Jensen and Kate Bridges for their computational expertise and innovative perspectives on this topic. Our collaboration was deeply educational and rewarding for me, and their contributions elevated the project to new heights I had not anticipated.

Our work was also transformed by the input of Dr. Shruti Naik and her lab at NYU Langone Medical Center. Dr. Naik and her team were incredibly generous with their data, protocols, time, and expertise, which enabled us to generate some of the most exciting data in this project, including the whole mount imaging of blood vessels in skin wound beds and the analysis of Langerhans cell-derived *Vegfa* in their single-cell RNA sequencing dataset.

I feel remarkably privileged to have worked with a team of fantastic scientists and friends throughout my time in the Horsley lab. When I joined the lab in 2016, the existing members, Dr. Brett Shook, Dr. Guillermo Rivera-Gonzalez, Dr. Rachel Zwick, Dr. Gabriella Grisotti, set such a high bar for how supportive, motivating, successful, and fun a lab environment could be. They each taught me about a unique area of epithelial cell biology, and my exposure to such a breadth of knowledge has made me a more curious, creative, and brave scientist. I especially want to acknowledge Brett's immense contributions to my scientific training. I feel like Brett saw potential in me and went above and beyond to invest in my development as a bench scientist, communicator, and collaborator. I am extremely proud of the work we have done together, and I hope to have more

opportunities to collaborate in the future. Additionally, I want to thank Rachel for being a shining example of an exceptional young scientist. I feel like many of my proudest accomplishments in this program were a product of my attempts to emulate Rachel, and she continues to inspire me today. I am also tremendously grateful to the more recent generations of Horsley lab scientists: Dr. Maria Fernanda (Nanda) Forni, Dr. Teresa Sandoval-Schaefer, Dr. Eunice Lozada Delgado, Dr. Abby Zieman, Dr. Kristyn Carter, Oliva Justynski, Elizabeth Caves, Ting Xu, Will Krause, Rebecca Pannone, and Armari Long. Each of you add to the stimulating and supportive scientific “niche” where I have been so lucky to grow and develop.

I have benefitted immensely from the mentorship and feedback of several communities at Yale, including my colleagues in the Department of Molecular, Cellular, and Developmental Biology (MCDB), the Yale Stem Cell Center, and the Yale Training Program in Genetics. I am very grateful for all the opportunities I have had to present my research, learn about others’ exciting discoveries, contribute to student committees to hire new faculty and promote diversity and inclusion in our community, and teach future generations of scientists and change-makers. Working as a teaching fellow with Drs. John Carlson and Joseph Wolenski was a highlight of my time in the Yale MCDB community, and I am so grateful for their sustained mentorship and friendship.

I had the immense privilege of participating in two internships run by the Yale Office of Cooperative Research, both of which connected me with a community of remarkable scientists who are passionate about translating

discoveries at the bench into breakthrough clinical therapies. During my time as a Canaan-Yale Fellow and a Blavatnik Associate, I had opportunities to connect with fantastic minds in both science and business, and this training cultivated my love for creative and rigorous science in a unique and inspiring way.

I want to express my gratitude, also, to Joseph Wolenski and Kenneth Nelson, for support and training in confocal imaging, flow cytometry, respectively.

My work was supported by the National Institutes of Health (NIH) T32 Training Grant, the Yale Training Programing in Genetics, led by Drs. John Carlson and Valerie Reinke. I also received financial support from a Predoctoral National Research Service Award granted by the National Institute of Arthritis and Musculoskeletal and Skin Disease at the NIH.

Finally, I want to express my deepest and sincerest gratitude to my friends and family, who together, form a bright ecosystem of love and support that has enabled me to thrive during even the most challenging phases of this process. I am so lucky to be surrounded with people who share or appreciate my passion for science, creativity, art (especially swing dancing!), innovation, big-picture thinking, and levity. I feel like I have an army of people cheering me on at all times, which has motivated me to take on big projects and challenges. I feel known, accepted, and loved for who I am, no matter how I show up on any particular day. Finally, I would not be here today without the unwavering support and guidance of my fantastic and wholly inspirational parents, Phyllis Rhodes and Brian Wasko.

Table of Contents

List of Figures and Tables

Figures

Tables

List of Nonstandard Abbreviations

ACKR: Atypical chemokine receptor
BMPR: Bone morphogenetic protein receptor
CD-: Cluster of differentiation
Cxcl-: C-X-C Motif Chemokine Ligand
DAMP: Danger-associated molecular pattern
DAPI: 4’,6-diamidino-2-phenylindole
DC: Dendritic cell
dDC: Dermal dendritic cell
DETC: Dendritic epidermal T cell
DTA: Diphtheria toxin alpha subunit
DTR: Diphtheria toxin receptor
DWAT: Dermal white adipose tissue
EC: Endothelial cell
ECM: Extracellular matrix
EdU: 5-ethynyl-2’-deoxyuridine
EGF: Epidermal growth factor
EpCAM: Epithelial cell adhesion molecule
ESM1: Endothelial cell-specific molecule 1
Fb: Fibroblast
FGF: Fibroblast growth factor
FSC: Forward scatter
HF: Hair follicle
HFSC: Hair follicle stem cell
IF: Interfollicular
IGF: Insulin-like growth factor
IL-: Interleukin
ILC: Innate lymphoid cell
iNOS: Inducible nitric oxide synthase
Kc: Keratinocyte
KGF: Keratinocyte growth factor
LC: Langerhans cell
Lin-: Lineage negative
MHCII: Major histocompatibility complex II
MMP: Matrix metalloproteinase
mRNA: Messenger RNA
mT/mG: tdTomato/membrane eGFP
Mø: Macrophage
PAMP: Pathogen-associated molecular pattern
PDGF: Platelet-derived growth factor

PECAM-1: platelet endothelial cell adhesion molecule 1
Pfn1: Profilin1
PGF: Placental growth factor
ROS: Reactive oxygen species
scRNA-seq: Single-cell mRNA sequencing
SSC: Side scatter
TGF-β: Transforming growth factor-β
TNFa: Tumor necrosis factor alpha
T_{reg}: Regulatory R cell
TRMs: Resident memory T cells
UV: Ultraviolet
VEGF: Vascular endothelial cell growth factor
Wnt: Wingless type

Chapter 1: Introduction

1.1. Introduction to Skin

Functions of skin. The skin is the largest single organ in the human body (Dąbrowska et al. 2018), and serves as the interface between our external and internal environments. Skin performs a myriad of protective and supportive functions which ultimately enable humans to thrive in diverse climates and withstand harsh environmental insults. Most notably, skin is a highly effective barrier, with both “outside-in” and “inside-out” functionality (Natsuga, 2014; Proksch *et al.* 2008). It provides “outside-in” protection by shielding underlying tissues from diverse types of damage, including physical assaults (UV irradiation and mechanical injury), microbial assaults (infection with bacteria, fungi, or viruses), and chemical assaults (irritants and allergens). It simultaneously provides “inside-out” protection by preventing water and electrolytes from escaping the body. In addition to its essential barrier function, the skin also plays important roles in temperature regulation (Charkoudian, 2003), sensation (Lumpkin & Caterina, 2007; Owens & Lumpkin, 2014; Roosterman *et al.,* 2006), immunity (Kobayashi, Naik & Nagao, 2019; Mansfield & Naik, 2020; Nguyen & Soulika, 2019; Sharma *et al.,* 2019), and the production of important metabolites (Bikle, 2011; Bocheva *et al*., 2022). Together, these functions enable us to navigate and interact with the outside world while maintaining homeostasis in our internal tissues.

Skin structure and composition. The structure and composition of skin are integral to its function. Skin possesses a diverse ecosystem of cell types organized into two distinct layers separated by a basement membrane: the outermost epidermal layer, and the underlying dermal compartment. Each of these layers possesses a unique cellular composition and extracellular matrix (ECM) environment, which imbues it with specialized functions.

Epidermis. The epidermis, the skin's outermost layer, is responsible for its water-tight barrier function. It is a stratified epithelium in which keratinocytes are the predominant cell type (Kretzschmar and Watt, 2014). The epidermis is in a state of constant regeneration, as keratinocytes from the basal layer act as adult stem cells and give rise to daughter cells that progressively differentiate to replenish the superficial layers (Alcolea and Jones, 2014). The epidermis also houses hair follicles, which contain a pool of epidermal stem cells (hair follicle stem cells, HFSC) that contribute to hair cycling, skin regeneration, and tumorigenesis (Arwert et al., 2012). These different subpopulations of keratinocytes coordinate their functions to perform and support biological functions in the epidermis, skin appendages, and underlying dermis.

In addition to keratinocytes, the mammalian epidermis contains other specialized cell types such as melanocytes, Merkel cells, and Langerhans cells (LCs) (Kobayashi, Naik, and Nagao, 2019). Recent studies have discovered the presence of additional immune cells, including innate lymphoid cells (ILCs) (Kobayashi et al., 2019) and resident memory T cells (TRMs) (Mueller and Mackay, 2016), in the epidermis. Mouse epidermis possesses a unique population

of resident γδ T cells, called dendritic epidermal T cells (DETCs), which participate in inflammation, wound healing, and tumor surveillance (MacLeod and Havran, 2011). Humans, however, lack these cells. Although these unique cell types are sparsely embedded in the dense network of epidermal keratinocytes, they contribute to important skin functions such as sensation (Merkel cells), metabolite synthesis (melanocytes), and immunity (LCs, ILCs, TRMs, & DETCs).

Dermis. Below the basement membrane that underlies the epidermis is the dermal compartment of the skin. The dermis is a thick, dynamic, extracellular matrix (ECM)-rich layer that is less densely cellular than the epidermis but contains a wider variety of cell types, including mesenchymal cells, endothelial cells (ECs), and immune cells. Fibroblasts are the dominant dermal cell type, and are critical for synthesizing and remodeling important ECM components (Stunova and Vistejnova, 2018). ECs are the building blocks of blood and lymphatic vessels, which form a complex network of small capillaries at the surface of the tissue feeding into larger vessels that run through the deeper tissue. Blood vessels supply the skin with essential oxygen, nutrients, and immune cells, while lymphatic vessels drain lymph fluid and immune cells (Varricchi et al., 2015).

The dermis also contains a plethora of immune cells, which patrol the tissue and mediate either homeostasis or immunity (Kobayashi, Naik, and Nagao, 2019). Several types of tissue-resident immune cells inhabit the dermis, including macrophages, dermal dendritic cells (dDCs), ILCs, and T cells (Pasparakis et al., 2014). In the absence of inflammatory or pathogen-associated signals, these cells primarily help maintain immune tolerance, and can also contribute to skin

functions, such as hair follicle cycling (Rahmani et al., 2020). When the skin becomes infected, skin-resident immune cells help quickly induce inflammation and coordinate a robust immune response involving both the innate and adaptive arms of immunity (Nguyen and Soulika, 2019). Interestingly, much like how immune cells contribute to classical skin functions, classical skin cells also contribute to immunity. Skin cells such as fibroblasts and keratinocytes shape immune responses directly by producing antimicrobial peptides, and indirectly by expressing inflammatory signals to shape immune cell function (Kobayashi, Naik, and Nagao, 2019; Kessler-Becker, et al., 2004).

Together, the cellular heterogeneity of the dermis imbues it with many qualities of an effective barrier, including physical strength and many defensive mechanisms to combat potential pathogenic intruders.

1.2. Skin Regeneration

It is critical that barrier tissues be highly regenerative in order to maintain their strength and quickly repair any damage they sustain. Skin has a remarkable capacity to regenerate, which is extremely valuable to human health since it is frequently challenged by external stressors and injuries.

Regeneration without injury. Skin has distinct biological programs for homeostatic regeneration and wound healing. As discussed in **Chapter 1.1**, the epidermis is in a constant state of self-renewal, with epidermal stem cells steadily giving rise to new keratinocytes that progressively differentiate as they move up

toward the surface of the skin (Alcolea and Jones, 2014). Additionally, the hair growth cycle is a unique model of tissue regeneration that cycles in three stages: quiescence (telogen), growth (anagen), and regression (catagen) (Plikus & Chuong, 2014). During this process, the skin undergoes massive remodeling, including dramatic growth of hair follicle (HF) keratinocytes, expansion of the dermal white adipose tissue (DWAT) (Festa et al., 2011), and finally, cell death and remodeling to restore homeostasis. This process is controlled by multiple cell types, including many that reside outside the HF. Adipocytes (Festa et al., 2011; Rivera-Gonzalez, Shook, and Horsley, 2014), dermal papilla cells (Plikus and Chuong, 2014), HF stem cells, and immune cells (Rahmani et al., 2020) all provide important signals to coordinate hair growth, which demonstrates the skin's capacity to integrate diverse and complex signals to facilitate tissue regeneration.

Wound healing. When skin is wounded, a cascade of events is initiated to mitigate the damage and generate new, functional tissue. Wound healing occurs through a series of temporally-overlapping and tightly regulated steps of inflammation, proliferation, and remodeling (Eming et al., 2014).

Inflammatory phase*.* After skin injury, inflammation is rapidly initiated by multiple proinflammatory signals, including factors released by degranulating platelets, danger-associated molecular patterns (DAMPs) released by damaged cells, and pathogen-associated molecular patterns (PAMPs) associated with infiltrating microbes (Eming et al., 2014). These signals help to recruit immune cells from the

circulation to the site of injury, where they can begin to clear and sterilize the wound bed. Neutrophils are among the first cells recruited to wounds and employ potent mechanisms to eradicate invading bacteria. These defense mechanisms include producing reactive oxygen species (ROS), phagocytosing bacteria, releasing cytotoxic granular contents, and in dire cases, ejecting neutrophil extracellular traps (NETs) (Phillipson and Kubes, 2019). While these behaviors are effective for killing bacteria and can help minimize bacterial spread into the body, they can also induce collateral damage, exacerbate inflammation, and delay regeneration (Phillipson and Kubes, 2019). Although this suggests that neutrophils' most significant contribution to wound healing is their ability to fight infection, there is mounting evidence that neutrophils perform anti-inflammatory functions as well. Efferocytosis (the phagocytosis of apoptotic cells) of dead neutrophils by macrophages drives macrophages to a pro-repair phenotype (Bosurgi et al., 2017). Additionally, a study of cardiac repair after myocardial infarction (which is considered a sterile injury) demonstrated that infiltrating neutrophils exhibited either a proinflammatory "N1" phenotype or an anti-inflammatory "N2" phenotype, similarly to macrophages (Ma et al., 2016). These studies highlight the complexity of the neutrophil response to tissue injury, and the need for future studies to further characterize their functions.

Following the early influx of neutrophils, Ly6C^{hi} monocytes are recruited to the wound from the circulation, where they become activated and differentiate into macrophages (Eming et al., 2007). During the early inflammatory phase of wound healing, the majority of these macrophages are polarized to a proinflammatory

phenotype and function to phagocytize cellular debris, apoptotic cells, and bacteria, as well as secrete inflammatory factors such as IL-1, IL-6, IL-12, TNFα, and inducible nitric oxide synthase (iNOS) (Barrientos et al., 2008; Landén et al., 2016; Wynn & Vannella, 2016). Additionally, macrophages produce cytokines to recruit more leukocytes to the site of injury. Depletion of macrophages during this phase diminishes the inflammatory response and can result in less efficient wound debridement and repair (Wynn & Vannella, 2016).

Together, infiltrating immune cells and local skin cells contribute to goal of the inflammatory phase of wound healing: to clear the tissue of pathogens and debris to make way for the generation of new, healthy tissue.

Proliferative phase*.* Once a lesion has been cleared of potentially pathogenic material, the wound bed macroenvironment switches from a pro-inflammatory to an anti-inflammatory phenotype and tissue regeneration is initiated (Landén et al., 2016). The broad functions of the proliferative phase of repair are to (I) reestablish the epithelial barrier, (II) generate granulation tissue, and (III) rebuild the vascular network. These processes are mediated by overlapping signals, many of which derive from macrophages.

Re-epithelialization requires that keratinocytes proliferate and migrate over the wound bed until they reform a contiguous epidermal layer. These migratory keratinocytes are generated from two pools of epidermal stem cells: basal interfollicular keratinocytes and hair follicle stem cells (HFSC) (Lau et al., 2009). Multiple molecular signals stimulate re-epithelialization, including chemical signals

(e.g. nitric oxide), growth factors (e.g. epidermal growth factor [EGF] family proteins, keratinocyte growth factor [KGF], insulin-like growth factor 1 [IGF1], and nerve growth factor [NGF]) and inflammatory cytokines (e.g. IL-1, IL-6, TNF) (Barrientos et al., 2008; Landén et al., 2016). These signals are produced by diverse cells, including platelets, macrophages, neutrophils, and fibroblasts.

Fibroblasts play a central role in shaping the wound ECM environment to promote the formation of granulation tissue during the proliferative phase of repair. Following injury, fibroblasts from many sources migrate into the provisional wound matrix (established by platelets during the clotting response) and then begin replacing it with new ECM (Stunova and Vistejnova, 2018). This new ECM serves as a scaffold upon which endothelial cells, immune cells, and additional fibroblasts can migrate into the wound to form robust granulation tissue. In addition to constructing the infrastructure on which cells navigate into wounds, fibroblasts also secrete a plethora of cytokines, chemokines, and growth factors that modulate proliferative processes (Stunova and Vistejnova, 2018).

Angiogenesis, the growth of new blood vessels from existing vasculature, is a vital component of the proliferative phase of tissue repair. Blood vessels are essential for skin health because they supply the tissue with critical oxygen, nutrients, and immune cells (Johnson and Wilgus, 2014). When skin is wounded, it is crucial that blood vessels are quickly restored in order to meet the elevated metabolic needs of the regenerating tissue, and to supply the tissue with circulating immune cells that promote regeneration (Martin and Gurevich, 2021). The paramount importance of angiogenesis to skin wound healing is highlighted by the

fact that defective revascularization is a phenotype shared by many types of chronic wounds, including diabetic ulcers (Martin and Gurevich, 2021).

Sprouting angiogenesis is a complex process that requires blood vessels to transition through phases of quiescence, activation, and resolution (Carmeliet and Jain, 2011). During homeostasis, blood vessels are maintained in a quiescent, structurally-stable state. Here, endothelial cells are tightly adhered to one another within mature vessels, which are structurally supported by a laminin- and collagen IV-rich basement membrane, as well as an outer layer of pericytes which promote vessel stability and EC survival (Johnson and Wilgus, 2014). When blood vessels are exposed to pro-angiogenic stimuli, ECs within the vessels begin to loosen their cell-cell connections. Additionally, pericytes start to detach from the outer vessel walls, and the basement membrane becomes susceptible to digestion by matrix metalloproteinases (MMPs) (Carmeliet and Jain, 2011). This loss of structural stability creates an opportunity for an endothelial cell to sprout from the existing vessel to initiate growth of a new vessel. The sprouting cell, called an endothelial tip cell, leads the outgrowth of the new vessel by sensing and migrating along a gradient of proangiogenic signals, such as vascular endothelial growth factor alpha (VEGFa) (Johnson and Wilgus, 2014). Neighboring ECs then take on the role of stalk cells, which proliferate and follow the migration of the leading tip cell, thus elongating the sprouting vessel (Carmeliet and Jain, 2011). During the resolution phase of angiogenesis, new vascular sprouts are consolidated, either by fusion of new spouts with neighboring sprouts to support blood flow, or by regression and

pruning of non-functional sprouts. (Carmeliet and Jain, 2011). Finally, quiescence is restored when new vessels reform their tight structural supports.

Since sprouting angiogenesis is highly multifaceted, this process can be influenced by diverse types of signals. Among the most commonly described angiogenic signals are growth factors (VEGFa, fibroblast growth factors [FGFs], and platelet-derived growth factor [PDGF]), cytokines (tumor necrosis factor alpha [TNFa], interleukin 1 beta [IL-1b]), and ECM-degrading proteases (MMP-2, MMP-9) (Ucuzian et al., 2010). The incredible complexity of angiogenic signaling provides functional redundancies that are evolutionarily advantageous, but make it challenging to induce angiogenesis with therapies that specifically target a single signaling pathway (Carmeliet and Jain, 2011).

Macrophages are intimately involved in all key proliferative wound healing responses, including re-epithelialization, angiogenesis, and fibrosis. As inflammation subsides, the overall population of wound macrophages shifts away from a pro-inflammatory phenotype and instead adopts an anti-inflammatory phenotype (Krzyszczyk et al., 2018; Wynn & Vannella, 2016). These pro-repair macrophages secrete abundant growth factors, anti-inflammatory cytokines, MMPs, and other signaling factors that instigate proliferative programs in surrounding skin cells. Depletion of macrophages during the proliferative phase of skin wound healing results in total abrogation of tissue repair (Shook et al., 2016; Wynn and Vannella, 2016), thus demonstrating that macrophages are indispensable for skin wound healing.

Remodeling phase*.* Following the successful formation of granulation tissue, the wound bed transitions into the remodeling stage of repair. In this phase, the newly regenerated skin tissue is incorporated into its surrounding skin environment by pruning excess cells and reorganizing the composition of the ECM (Stunova and Vistejnova, 2018). Myofibroblasts, endothelial cells, and immune cells gradually undergo apoptosis, and the tissue takes on a mature, “acellular” phenotype that resembles naive skin (Gonzalez et al., 2016). Additionally, the majority of the type III collagen deposited during earlier stages of repair is replaced by type I collagen, which slowly accumulates cross links that provide added strength to the tissue (Stunova and Vistejnova, 2018). Unlike the previous stages of repair, wound remodeling occurs at a much slower rate, and can occur over the span of months or years.

1.3. Langerhans cells

LCs are considered sentinels of the body because they are among the first line of defense against invading molecules and microorganisms. As introduced in **Chapter 1.1**, LCs reside in the epidermis, where they continually probe their surroundings for signs of damage or infection (Kobayashi, Naik & Nagao, 2019). LCs can be distinguished from dermal DCs by their localization in the epidermis and high co-expression of the cell surface markers Langerin (CD207), major histocompatibility complex class II (MHC-II), and EpCAM (Rajesh et al., 2019). Like other classes of DCs, LCs express high levels of pattern recognition receptors, such as Toll-like receptors (TLRs) and C-type lectin receptors, which enable them

to efficiently detect pathogen- and damage-associated molecular patterns (PAMPs and DAMPs) and initiate an appropriate immune response (Flacher et al., 2006; Figdor et al., 2002; Nagao et al., 2009; Rajesh et al., 2019). Upon detection of a danger-associated molecule, LCs function as professional antigen presenting cells, migrating to draining lymph nodes and presenting the antigenic material to naive lymphocytes to elicit a T cell response (Clausen and Kel, 2010; Bursch et al., 2007). LCs also direct immune cell activation through paracrine signaling. Secretion of the inflammatory cytokine interleukin-15 (IL-15) by LCs in humans has been shown to prime naive CD8+ T cells to become active cytotoxic T lymphocytes (Romano et al., 2012). In addition to their potent immunogenic potential, LCs function to dampen certain immune responses and promote an anti-inflammatory state in the skin. LCs have been shown to protect mice against allergic contact dermatitis (Gomez de Agüero et al., 2012) and autoimmune encephalomyelitis (Bynoe et al., 2003) through the induction of regulatory T (T_{reg}) cells. Although it has been well established that LCs recognize and respond to epidermal insults, there has been a significant gap in our understanding of how these cells contribute to specific wound healing processes.

Langerhans cells in wound healing. Different studies have proposed opposing roles for LCs in skin repair. A wound healing study using *muLangerin*-DTR mice recently reported that depletion of all Langerin+ cells resulted in accelerated wound healing. Here, the authors suggest that LCs may hinder wound healing processes while acknowledging that the mouse model they used does not

specifically deplete LCs. (Rajesh et al., 2020). In *muLangerin*-DTR mice, the receptor for diphtheria toxin is under the control of the mouse promoter for *langerin*, which is expressed by both LCs and dermal Langerin+ DCs (Bobr et al., 2010). Therefore, treatment of *muLangerin*-DTR mice with diphtheria toxin depletes both LC and dDC populations. Studies that have compared the consequences of broad Langerin+ cell depletion to LC-specific depletion have shown that LCs and Langerin+ dDCs play opposing roles in several inflammatory contexts, such as contact hypersensitivity reactions (Bobr et al., 2010), response to genetic immunization (Nagao et al., 2009), and infection with Candida albicans (Igyártó et al., 2011). Therefore, LC-specific depletion models, such as *huLangerin*-DTA mice (in which expression of the active alpha subunit of diphtheria toxin is driven by the human *langerin* promoter) (Kaplan et al., 2005), should be used to accurately dissect the roles that LCs play in wound healing.

Clinical data from diabetic patients suggest that LCs may promote skin repair. In a study that examined LCs in diabetic foot ulcers, a prevalent type of chronic wound, investigators found that patients whose wounds contained a higher density of LCs ultimately went on to have better healing outcomes four weeks later (Stojadinovic et al., 2013). This observation is consistent with LCs acting locally within skin wounds to promote regeneration. However, these data are purely correlational, and controlled studies are needed to characterize the contributions of LCs to skin wound healing.

Chapter 2: Identification of angiogenic regulators in skin

Note: The research in Chapters 2, 3, and 4 is being prepared as a manuscript for publication as follows:

Renee R. Wasko, Kate Bridges, Rebecca Pannone, Ikjot Sidhu, Yue Xing, Shruti Naik, Kathryn Miller-Jensen, and Valerie Horsley. Langerhans cells are an essential component of the angiogenic niche during skin repair.

Author contributions: The single-cell analyses reported in this chapter were performed by our collaborators, with our input. The analysis of the GSE142471 dataset was performed by Kate Bridges. The GSE166950 dataset was generated by Dr. Yue Xing, PhD, and was analyzed by Ikjot Sidhu.

Introduction

As reviewed in **Chapter 1**, angiogenesis is essential for the successful repair of skin wounds. Blood vessels supply the skin with oxygen and nutrients, which are critical for the fundamental cellular processes that support tissue function. Blood vessels also provide a route for circulating immune cells to access the skin, where they contribute to wound debridement, clearance of pathogens, and secretion of repair signals.

Wound-induced angiogenesis is highly complex and our current understanding of the signals that control it is not comprehensive. Diverse cell types, including fibroblasts, keratinocytes, and macrophages, have been shown to function as key components of the skin's angiogenic niche, each producing a variety of signals that promote wound revascularization (Eming et al., 2016). Among these angiogenic signals are well-studied growth factors, including vascular endothelial growth factors (VEGF), fibroblast growth factors (FGF),

platelet-derived growth factors (PDGF), and transforming growth factor beta (TGF-b) family members. Additionally, other classes of molecules, such as cytokines, extracellular matrix (ECM) components, cell adhesion molecules, and matrix metalloproteinases (MMP), have also been shown to contribute to wound-induced angiogenesis (Barrientos et al., 2008; Wynn and Vannella, 2016).

Despite the characterization of multiple cellular and molecular drivers of angiogenesis, there is a dearth of therapeutics that effectively promote angiogenesis in human wounds. Notably, therapies targeting VEGF signaling, which has been extensively validated as a potent inducer of angiogenesis, have proven unsuccessful for improving clinical healing outcomes in diabetic wounds (Giacca and Zacchigna, 2012; Johnson and Wilgus, 2014). The fact that targeting a potent angiogenic signaling pathway is insufficient to improve revascularization in patient wounds highlights the complexity of skin angiogenesis and illustrates the importance of expanding our understanding of the angiogenic niche.

In this chapter, we characterize the angiogenic niche in mouse skin at the transcriptomic level. Using single-cell RNA sequencing (scRNA-seq) data from wounded and unwounded skin, we apply computational methods to uncover potential signaling networks between endothelial cells (EC) and other cells in the wound microenvironment.

Results

Angiogenesis is initiated at the beginning of the proliferation phase of wound healing as indicated by immunostaining with CD31 (platelet endothelial cell

adhesion molecule, PECAM-1) (Newman et al., 1990) antibodies of skin sections of wounds 3, 5, and 7 days after injury (Fig. 1)(Eming et al., 2007). To identify factors that contribute to the angiogenic niche within skin wounds, we analyzed scRNA-seq data from mouse skin wounds at the beginning of the proliferative phase of repair (Haensel et al., 2020). By training a neural network to identify cell types based on expression of established marker genes (Fig. 2A)(following the approach from Kumar et al. 2018), we classified 11 broad cell types in the scRNA-seq data (Haensel *et al.*, 2020), including classes of immune cells, keratinocytes, fibroblasts, endothelial cells, and skeletal muscle cells (Figs. 2B and 2C). Next, we examined the expression of known angiogenic ligands (*VEGFA, TNF, Ptgs1, and Fn1*)(Adams and Alitalo, 2007) across the 11 cell clusters in wounded skin compared to non-wounded skin (Fig. 3A-D). We found that several known proangiogenic factors are expressed in non-wounded and wounded skin at varying levels, including *Vegfa* (Fig. 3A, 3C-D). Multiple cell types express *Tnf*, *Vegfa*, and *Ptgs1*, and fibroblasts predominantly express *Fn1* (Fig. 3C-D), indicating an unappreciated complexity to the early angiogenic niche in skin wounds.

To gain a comprehensive picture of the angiogenic niche within skin wounds, we utilized the NicheNet algorithm, which infers ligand binding from patterns of target gene expression in receiving cells (Browaeys et al., 2020). Specifically, we sought to infer signaling to ECs from the other classes of cells identified in the scRNA-seq data. We defined target genes in ECs as genes that were differentially expressed ($\log_2$FC > 0.25 and adjusted p-value < 0.05) in ECs after wounding as compared to non-wounded conditions. Correlation of observed

expression of these EC target genes against NicheNet's prior model implicated 202 potential ligands (i.e. angiogenic factors) as driving patterns in EC gene expression after wounding (Fig. 4A). Fibroblasts express the most angiogenic factors at 53, and skeletal muscle cells expressed the fewest at 8 angiogenic mRNAs (Fig. 4B). Among the immune cell populations, macrophages expressed the most angiogenic mRNAs (Fig. 4B), which is consistent with their well-established role driving angiogenesis in skin wounds (Koh et al., 2013). Surprisingly, we found that dendritic cells, LCs, and T cells expressed a similar number of angiogenic mRNAs as keratinocytes (Fig. 4B), which have been shown to be a major regulator of angiogenesis during wound healing (Rossiter *et al.*, 2004).

To characterize the cellular interactions between endothelial cells and other cell types within skin wounds, we focused on ligands expressed by specific cell types and used NicheNet to predict the potential for these ligands to interact with receptors expressed by ECs (i.e. interaction potential), and their potential to activate EC downstream target genes (i.e. regulatory potential) within skin wounds (Fig. 5A-D). We found that fibroblasts (including fibroblast and myofibroblast subsets) upregulated several ligands that are predicted to interact with integrins, atypical chemokine receptors (ACKRs), bone morphogenetic protein receptors (BMPR), and fibroblast growth factor (FGF) receptors, and activate several genes in endothelial cells (Fig 5A). Keratinocytes (including hair follicle (HF) and interfollicular (IF) subsets) expressed agonists for Wnt and Notch signaling, and cytokine receptors that are predicted to activate several signaling factors and

extracellular matrix gene expression in endothelial cells (Fig. 5B). Macrophages upregulated multiple angiogenic cytokines (*TNF, Il10, Il1a*) and additional ligands that induced ECM and other signaling factors (Fig. 5C). Endothelial receptors were predicted to be activated by distinct ligands produced by each cell type, suggesting that each cell within the repairing wound contributes uniquely to the angiogenic niche. Yet, these receptors are predicted to activate several similar target genes to control angiogenesis including *Fos, Cxcl12, Col4a2,* and *Col18a1*. Together, these data provide a map for the multiple interactions that may drive early events in angiogenesis within skin wounds (Fig. 5D).

Langerhans cells upregulate angiogenic mRNAs in skin wounds

We were surprised by the expression of several angiogenic mRNAs in LCs, a subset of phagocytic immune cells resident in the epidermis (Fig. 3C). Others have shown that depletion of all langerin+ cells, which includes LCs and a subpopulation of dermal dendritic cells, resulted in enhanced wound repair in mice (Rajesh et al., 2020). CD11c+ dendritic cells have been implicated in the repair of burn wounds in studies that depleted CD11c+ cells but not LCs using genetics mouse models (Vinish et al., 2016). Thus, we sought to determine if LCs function in skin wound repair, and specifically in angiogenesis.

Consistent with LCs playing a unique role in wound repair compared to other DC populations (Vinish et al., 2016), LCs cluster distinctly from dermal DCs, macrophages, and lymphocytes in unwounded and wounded samples after injury (Fig. 2C). This distinct clustering of LCs compared to dermal DCs and other

immune cells also occurred when immune cells were enriched via FACS purification based on CD45 expression (Fig. 6A-D; GSE166950), and the expression of the angiogenic factor *Vegfa* was noted in LCs in non-wounded and wounded skin (Fig. 6E). NicheNet also revealed 14 angiogenic mRNAs for which LCs are the dominant source in non-wounded and wounded skin, including cytokines, cytoskeletal modulators, and cell adhesion molecules (Fig. 7A). During tissue repair, the LC-derived ligands interact with several receptors and target genes that are upregulated by wound derived ECs (Fig. 7B-C). In particular, LC expression of C-X-C Motif Chemokine Ligand 16 *(Cxcl16)*, Protocadherin 7 *(Pcdh7), Vegfa*, and Placental growth factor (*Pgf*) mRNAs are predicted to bind to multiple receptors upregulated by ECs in skin wounds. Furthermore, LC ligands are predicted to activate *Fos,* Profilin1 *(Pfn1), and Pecam1* expression by ECs, which contribute to EC proliferation and migration (Adams and Alitalo, 2007; DeLisser et al., 1997; Fan et al., 2012; Sun et al., 2017).

LCs also significantly upregulated 577 genes in response to injury (Fig. 8A; p-adj value < 0.05), and gene ontology analysis of the changed genes in LCs during wound repair revealed that angiogenesis was a major category (Fig. 8B, Table 1). Furthermore, several angiogenic genes were upregulated by LCs after injury (Fig. 8C). Mapping the top ligands predicted to interact with EC receptors during wound healing, we observed that LCs are a significant source of these interactions, along with fibroblasts, keratinocytes, and macrophages (Fig. 7D).

Data Summary and Conclusions

Together, these data provide a transcriptional map of the angiogenic niche in the skin. Our analyses captured known angiogenic signaling axes (e.g. expression of *Tgfb3* and *Fgf1* in fibroblasts, and *Vegfa*, *Il10*, and *Tnf* in macrophages), as well as illuminated many new potential regulators of skin angiogenesis. I was excited to learn that expression of angiogenic mRNAs was not limited to a few cell types; rather, we observed that each cell type in our analysis transcribed a unique combination of angiogenic genes, thus contributing to the complexity and heterogeneity of the angiogenic niche. I hope that this transcriptomic characterization of angiogenic factors in skin wounds serves as a useful tool for further studies of angiogenesis in complex tissues.

I was intrigued by the fact that several immune cells, particularly LCs, expressed a similar number of angiogenic mRNA species as keratinocytes, which are known to promote revascularization after injury. Upon further investigation, we discovered that LCs express a unique program of angiogenic ligands and respond to skin wounding by upregulating a network of genes implicated in angiogenesis and vascular development. These data carve out a unique place for LCs within the broader angiogenic landscape in the skin, and highlight their potential importance for the regeneration of blood vessels after injury.

Although single-cell transcriptomic analyses are a powerful tool for studying biological changes within complex tissues, it is important to acknowledge their limitations. Our data do not provide insight on protein levels or activation of downstream signaling pathways, which could be important for understanding the

de facto contributions of each cell type to angiogenesis. Although further mechanistic studies are required to fully understand the angiogenic potential of our predicted cell-derived ligands, our work captures and highlights the complexity of the angiogenic niche, providing valuable context for future work. Furthermore, the complexity of this system may help explain why therapies that target a singular signaling pathway are inadequate to rescue defective revascularization in humans. I hope that our work may therefore inform the design of future therapies to treat chronic wounds.

Chapter 3: Langerhans cells localize at the regenerating edges of skin wounds

Introduction

As introduced in **Chapter 1**, LCs are long-lived, tissue-resident immune cells that help maintain tissue homeostasis and defend against pathogens. LCs are considered “sentinel” cells because they (I) reside in the skin’s epidermal layer, which interfaces with the outside world, (II) patrol their microenvironment for signs of tissue damage or infection, and (III) shape local T cell responses accordingly to the environmental cues they encounter (Clausen and Kel, 2010). LCs also migrate through the dermis to skin-draining lymph nodes (SDLN) at a slow rate during steady-state conditions and more robustly in response to inflammatory stimuli, where they can then present antigen to naive T cells (Clausen and Kel, 2010; Bursch et al., 2007).

Since LCs are sensitive to changes in their environment and can respond by migrating into the dermis, we were keen to investigate where LCs localize during wound healing. We were particularly interested in illuminating the spatial relationship of LCs and blood vessels, given that our transcriptomic analysis in **Chapter 2** suggests that LCs produce angiogenic signals during wound healing. In this chapter, we use flow cytometry, genetic mouse models, immunofluorescence staining, and confocal microscopy of whole mount wound beds to elucidate where LCs localize during skin repair.

Results

Langerhans cells localize at the edges of wounds in the dermis and epidermis

Langerhans cells are seeded in the skin during embryonic development (Hoeffel et al., 2012), and are replenished by low rates of local proliferation (Merad et al., 2002), or by bone marrow-derived precursors that migrate into the epidermis and differentiate into LCs (Seré, et al., 2012). In consonance with prior analysis of the location of langerin+ cells in skin wounds (Rajesh et al., 2020), we found a significant increase in MHCII+, CD45+ LCs within the healing epidermis in skin wounds from days 1 to 5 (Fig. 9A-B).

To precisely and accurately define the spatial location of LCs in mouse wounds, we generated an inducible fluorescent reporter mouse in which membrane-associated GFP can be activated in LCs with high specificity by crossing *huLangerin*-CreER mice (Bobr et al., 2012) to mT/mG dual fluorescent reporter mice (Muzumdar et al., 2007) to generate the *huLangerin*-CreER;mT/mG (LC-iGFP) mouse model (Fig. 10A). Low dose tamoxifen treatment of these mice induces the nuclear localization of Cre recombinase in LCs but not in langerin+ dermal dendritic cells (dDCs) (Bobr *et al.*, 2012) (Fig. 10C). Indeed, when we treated LC-iGFP mice with tamoxifen (Fig. 11A), we noted that 98% of EpCAM+, CD45+, MHCII+ LCs were labeled (Fig. 10B). Thus, this mouse model labels LCs specifically, which is consistent with the specific activity of the *huLangerin* promoter in LCs (Kaplan et al., 2005). Furthermore, this mouse model allows specific labelling of resident LCs by administering tamoxifen (which induces LC-specific

GFP expression) prior to injury, thereby only labeling the pool of fully-differentiated LCs present in naive skin.

Given the specificity and high efficiency of LC labeling in LC-iGFP mice, we examined the location of GFP+ cells in skin wounds 1, 3, 5, and 7 days post-injury (Fig. 11A-C). At each time point, we observed LCs in the epidermis at the edges of skin wounds and in adjacent skin (Fig. 11C). At later stages of healing, 5 and 7 days after injury, we also observed LCs in the newly-regenerated epidermis (Fig. 11C). GFP+ LCs were also present in the dermis in wound-adjacent skin, at wound edges, and later, in the wound bed (Fig. 11D).

Langerhans cells are concentrated at the growing tips of regenerating blood vessels during wound repair.

Since the main genes induced by LCs after injury were associated with angiogenesis (Fig. 8B), we sought to define the spatial relationship between LCs and ECs during skin repair. Using LC-iGFP mice, we injected tamoxifen daily for 3 days prior to wounding to induce GFP expression in LCs (Fig. 11A), and then co-stained wound beds for CD31+ endothelial cells. In cross sections of skin wounds, LCs in the dermis were near ECs 3 and 5 days after injury (Fig. 12A). To examine the spatial relationship between LCs and sprouting vessels in the three-dimensional tissue, we performed tissue clearing of 3-day wound beds of LC-iGFP mice and immunostained the whole mount tissue with antibodies against CD31 and GFP (Fig. 12B). Imaging throughout the depth of the skin tissue provided a view of the regenerating endothelial vessels as the tip cells enter the repairing

dermal compartment of the wound bed (Fig. 12B). We noted that the middle of the wound bed contained GFP+ cells that were likely resident in the re-epithelizing keratinocyte layer (Fig. 12E). Interestingly, we found that many LCs were clustered at the leading tips of the repairing endothelial vessels (Figs. 12C-D, 13A-C). Additionally, a few LCs were also observed along the length of vessels (Fig. 12C-D). These data indicate that LCs are spatially poised to promote dermal angiogenesis during wound healing.

Data Summary and Conclusions

Here, we demonstrate that LCs contribute to the makeup of the wound microenvironment in both the dermal and epidermal compartments of the skin. Using inducible fluorescent reporter mice, we were able to show that mature LCs labeled prior to injury are positioned at the epidermal edges of wounds during the inflammatory (1 and 3 days post-injury), proliferative (5 days post-injury), and remodeling (7 days post-injury) stages of repair. We also found that lineage-traced LCs migrate into the newly regenerating epithelium. These findings provide rationale for future studies that examine how the LC network in the epidermis is restored after injury. Previous work has shown that in response to inflammatory insults, monocytes infiltrate the epidermis and differentiate into LCs, replacing the resident LCs that migrated to the skin draining lymph nodes (Seré et al., 2012). It would be fascinating to use our LC-iGFP inducible fluorescent reporter mice to perform lineage tracing experiments to determine (I) if the epidermal LC network is fully restored after injury, and (II) if LCs in newly regenerated skin originate

predominantly from the migration/proliferation of local LCs, or from the infiltration and differentiation of monocyte-derived precursors.

Additionally, we were fascinated to learn that LCs localize at the dermal edges of wounds, as well as within the granulation tissue. These observations pose interesting questions as to whether LCs integrate into new dermal tissue and become a lasting component of the cellular milieu. The presence of LCs in the dermis 7 days after injury also poses the question of whether LCs contribute to the remodeling phase of wound healing. We are interested in designing future studies that examine later time points after injury with scRNA-seq and histological assays to interrogate if LCs contribute to dermal remodeling after injury.

Using tissue clearing and confocal microscopy, we were able to visualize the spatial relationship between LCs and blood vessels in three-dimensional (3D) skin tissue. These data not only aligned with our histological observations in wound cross-sections, but also enabled us to clearly visualize the 3D network of blood vessels in the skin, and where LCs localize in relation to wound-associated vessels. We were excited to observe that LCs concentrate at the leading tips of regenerating blood vessels, where endothelial stem cells (tip cells) are known to reside (Johnson and Wilgus, 2014). Here, we believe LCs are poised to interact with endothelial stem cells via paracrine or contact-mediated signaling. To build on these findings, I would label endothelial tip cells by staining for endothelial cell-specific molecule 1 (ESM1) and then capture high magnification Z-stack images of wound edges to determine the precise special relationship between LCs and tip cells. Nevertheless, the spatial proximity between LCs and blood vessel tips

positions LCs to deliver angiogenic signals to endothelial cells and promote angiogenesis during wound healing.

Chapter 4: Langerhans cells are essential for skin revascularization and repair

Introduction

In **Chapter 1**, I summarize several studies that have postulated contradictory roles for LCs in skin repair. For example, Stojadinovic *et al.* (2013) observe that the density of LCs in human diabetic foot ulcers correlates positively with successful healing outcomes, and suggest that LCs may promote wound healing. Conversely, Rajesh *et al.* (2020) report accelerated wound healing in mice that had been depleted of all langerin+ cells, which includes LCs and dermal langerin+ DCs, and postulate that LCs may dampen regenerative responses. While these studies each provide the field with unique insight, they lack the proper tools and experimental design to specifically interrogate the role of LCs in skin repair. This gap in our understanding highlights the need for careful investigation of how LCs shape wound healing processes.

The data presented in **Chapters 2** and **3**, demonstrate that LCs express angiogenic genes in response to injury and are spatially poised to deliver signals to blood vessels in the wound niche. In this chapter, I demonstrate a functional role for LCs in skin repair. To specifically target LCs, I utilized a genetic mouse model in which LCs are specifically and constitutively depleted while langerin+ dermal DCs are spared. In these LC-depleted mice, I used tissue histology and flow cytometry to measure multiple aspects of wound healing, including revascularization, fibroblast repopulation, re-epithelialization, and immune cell

infiltration. I also took advantage of tissue clearing and confocal microscopy to visualize the 3D architecture of regenerating blood vessels in wounds from LC-depleted mice. With this, I characterized how wound healing is defective in the absence of LCs.

Results

Multiple facets of skin repair are defective in LC-depleted mice

Since LCs are present in regions of skin wounds undergoing repair (Figs. 11-13), we sought to determine if LCs contribute to skin wound healing, and particularly to angiogenesis. To this end, we analyzed tissue repair in a mouse model that specifically lacks LCs using *huLangerin*-DTA (*huLang*-DTA) mice, in which the promoter sequence for the human *langerin* gene drives expression of diphtheria toxin, resulting in constitutive and specific ablation of LCs without impacting langerin+ dDCs (Kaplan et al., 2005)(Fig. 14A-C). Importantly, we did not detect any changes in skin structure in uninjured adult *huLang*-DTA mice compared to control littermates (Fig. 14D). After injury, we noted that the epidermis bordering 1-day wounds in littermate control mice contained ~2.5% LCs, LCs were almost entirely depleted in *huLang*-DTA+ mice (Fig. 14A-B).

To examine skin wound repair in the absence of LCs, we analyzed skin wounds at various time points after injury in *huLang*-DTA mice. Interestingly, LC-deficient mice did not display defects in the inflammatory response 3 days after injury. LC-deficient mice possessed similar numbers of monocytes, macrophages, and T cells in 3-day wounds compared to DTA- littermate controls (Fig. 15A-E).

Thus, despite the importance of the recruitment of immune cells during the inflammatory phase of healing (Eming *et al.*, 2014) and the proposed role for LCs in this process (Igyarto and Kaplan, 2010), inflammatory cell recruitment after skin injury proceeded normally in the absence of LCs (Fig. 15B-E), as indicated by similar monocytes and macrophages numbers and polarization in *huLang*-DTA mice compared to control mice (Fig. 15B-E). Furthermore, we did detect slightly more T cells as a percentage of total immune cells (Fig. 15D), but the absolute number of T cells at day 3 after injury was not significantly different between the DTA+ and DTA- samples (Fig. 15E). Therefore, this difference in relative T cell abundance is likely due to the slightly reduced numbers of CD45+ cells in DTA+ mice (Fig. 15B-C).

Examination of the proliferative phase of wound healing revealed that *huLang*-DTA+ mice exhibited profound regenerative defects compared to littermate controls. Histological analysis of hematoxylin and eosin-stained sections of skin wounds revealed that wounds of *huLang*-DTA+ mice were wider and thinner than control mice (Fig. 16A). To analyze which cell types were impaired in *huLang*-DTA+ mouse wounds, we analyzed the repair of keratinocytes, ECs, and fibroblasts. While keratinocyte re-epithelialization was variable in control mice, no significant defect was detected in the percent of wound area covered by in *huLang*-DTA+ mouse wounds compared to control mice (Fig. 16J). However, FACS analysis of cells within skin wounds revealed a significant reduction in the number of CD31+ ECs (Figs. 16C-D) and CD29+ fibroblasts (Fig. 16E) in the wound beds of *huLang*-DTA+ mouse wounds compared to control mice. Histological analysis

of the localization of ER-TR7+ fibroblasts within 5 day wound beds revealed a ~70% reduction in fluorescence within skin wounds depleted for LCs (Fig. 16H-I). Similarly, *huLang*-DTA+ mice displayed a 4-fold decrease in fluorescence of CD31+ EC compared to wound beds of control mice (Fig. 16F-G). Together, these data suggest that LCs directly promote proliferative repair processes, which are critical for efficient wound repair.

Langerhans cells are critical for angiogenesis during wound repair.

To investigate the angiogenic repair defects in LC depleted mice in more detail, we examined the vascular network in *huLang*-DTA mice. Naive skin of LC-depleted mice displayed normal vasculature organization (Fig. 17A) as indicated by whole mount imaging of cleared wound beds immunostained with antibodies against CD31. Control wounds displayed clear signs of blood vessel repair mechanisms, including higher coverage of the wound bed with CD31+ blood vessels and thick vessels concentrated distally to the wound bed (Fig. 17B). In contrast, LC-depleted wounds exhibited stunted vessel growth at the edge of the wound bed and lacked clusters of large vessels (Fig. 17B). Examining the tip cells, which extend and proliferate to form new blood vessels at the leading edge of angiogenesis, we noted a thick density of overlapping tip cells clustered at the leading edge of the sprouting angiogenic front in control mice (Fig. 17B-C). However, in mice lacking LCs, tip cells were distant from neighboring tip cells at the leading edge of the blood vessel front, and the vessels appeared thinner and sparser than the wounds control mice (Fig. 17B-C).

To determine if LCs are required for proliferation of endothelial cells after injury, we pulsed *huLang*-DTA mice with EdU during the height of EC proliferation (3 and 4 days after injury) to label proliferating cells (Fig. 18A), and analyzed CD31+, EdU+ cells 5 days after injury using flow cytometry. Compared to control samples, wounds from LC-depleted mice contained significantly fewer total EdU+, CD31+ endothelial cells (Fig. 18B-C). Immunostaining of skin wound sections from mice pulsed with EdU confirmed that CD31+ cells in LC-depleted mice displayed reduced proliferation during this critical time for angiogenesis associated with tissue repair (Fig. 18D). Interestingly, fibroblasts and CD45+ immune cells did not display significant changes in proliferation at day 3 in *huLang*-DTA mice compared to control mice (Fig. 18E-F). Taken together, our data provide evidence that LCs are necessary for angiogenesis in skin wounds.

Data Summary and Conclusions

Here, I have shown that mice constitutively lacking LCs exhibit severe wound healing defects. Despite the fact that the skin of LC-depleted mice appeared phenotypically normal prior to injury, *huLang*-DTA+ wounds at the height of the proliferative phase of repair had significantly reduced fibroblast repopulation and revascularization compared to controls, as demonstrated with flow cytometry and histological analyses. Interestingly, we did not observe defects in re-epithelialization nor in immune cell recruitment in the absence of LCs, meaning that LCs communicate with specific cell types during wound healing. The fact that macrophage number and polarization were not significantly different in *huLang*-

DTA+ wounds also suggests that defects to angiogenesis and fibroblast repopulation in these mice were not a consequence of aberrant macrophage recruitment. It is important to note, however, that our characterization of macrophage populations is based on labeling cell surface markers, which does not fully represent cell function. It would be interesting to do a deeper characterization of the immune cell populations in LC-depleted wounds by performing mass cytometry (labelling for intracellular and secreted proteins) and secretomic analyses.

Our data also do not specifically address the question of whether the fibroblast phenotype and the angiogenic defects are connected, or if LCs signal to each cell type separately. This is a complicated relationship to tease apart, and should be addressed in future studies with methods such as single-cell transcriptomic and proteomic analyses to characterize changes within fibroblast and endothelial cell populations, and characterization of the ECM environment in *huLang*-DTA wounds. However, our data collectively enable us to conclude that LCs promote skin regeneration after injury.

Our whole mount analysis of the vascular network in *huLang*-DTA wounds provided a striking view of the angiogenic defects in LC-depleted skin. Not only did we observe less blood vessel coverage in *huLang*-DTA+ wounds, but also the three-dimensional network of vessels appeared sparser, with fewer vessel tips extending into the wounds. Furthermore, it is likely that vessel remodeling is defective in *huLang*-DTA+ wounds compared to controls. While the vessels at the edges of LC-depleted wounds were predominantly small and thin, we saw many

examples of small vessels merging into larger vessels in the control wounds. These observations in the tissue structure were supported by our EdU incorporation data, which demonstrate that endothelial cell proliferation is defective in *huLang*-DTA+ wounds. In this experiment, we maximally labeled proliferating cells by saturating the system with EdU (intraperitoneal injections twice per day) during the height of EC proliferation. Under these conditions, ECs in LC-depleted wounds incorporated significantly less EdU than in controls. Together, this illustrates that when LCs are absent from skin tissue, blood vessels do not receive the signals necessary to induce proliferation and assembly into a functional vascular network after wounding.

I was particularly excited to see the striking differences between the vasculature in *huLang*-DTA+ vs. control wounds, and I believe these data invite future studies to more thoroughly characterize how LCs shape angiogenesis. It would be fascinating to examine vessel maturation at different timepoints throughout repair by labelling cell markers that distinguish capillaries, veins, and arterioles. It would also be interesting to capture higher magnification images of the wound-edge vasculature and use image analysis software to quantify features such as average vessel width and number of branch points to further describe the defect. These assays could further our understanding of both LC biology and skin angiogenesis, more broadly.

Figures and Tables

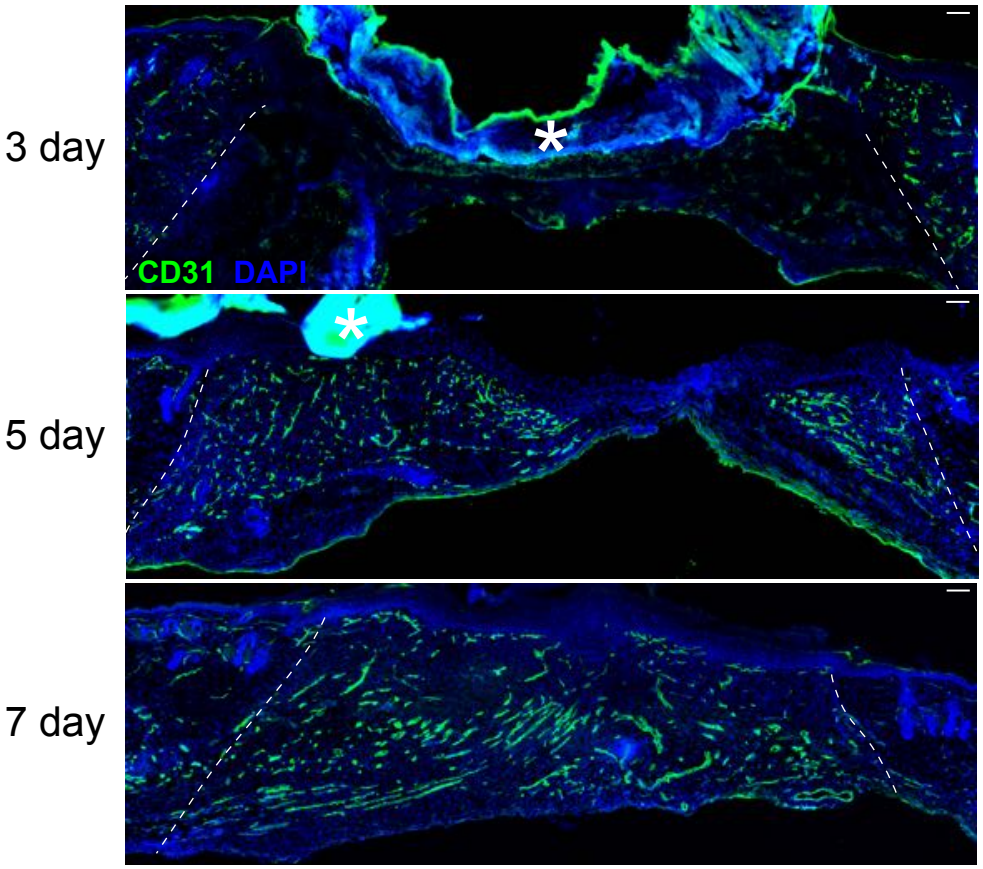

Figure 1: Angiogenesis occurs during the proliferative phase of wound healing. Images of CD31 immunostaining (green) and DAPI-stained nuclei (blue) in cross-sections of 3-, 5-, and 7-day wound beds. The white dashed lines delineate wound edges. Asterisks (*) indicate non-specific staining of scab. Scale bars, 100 μm.

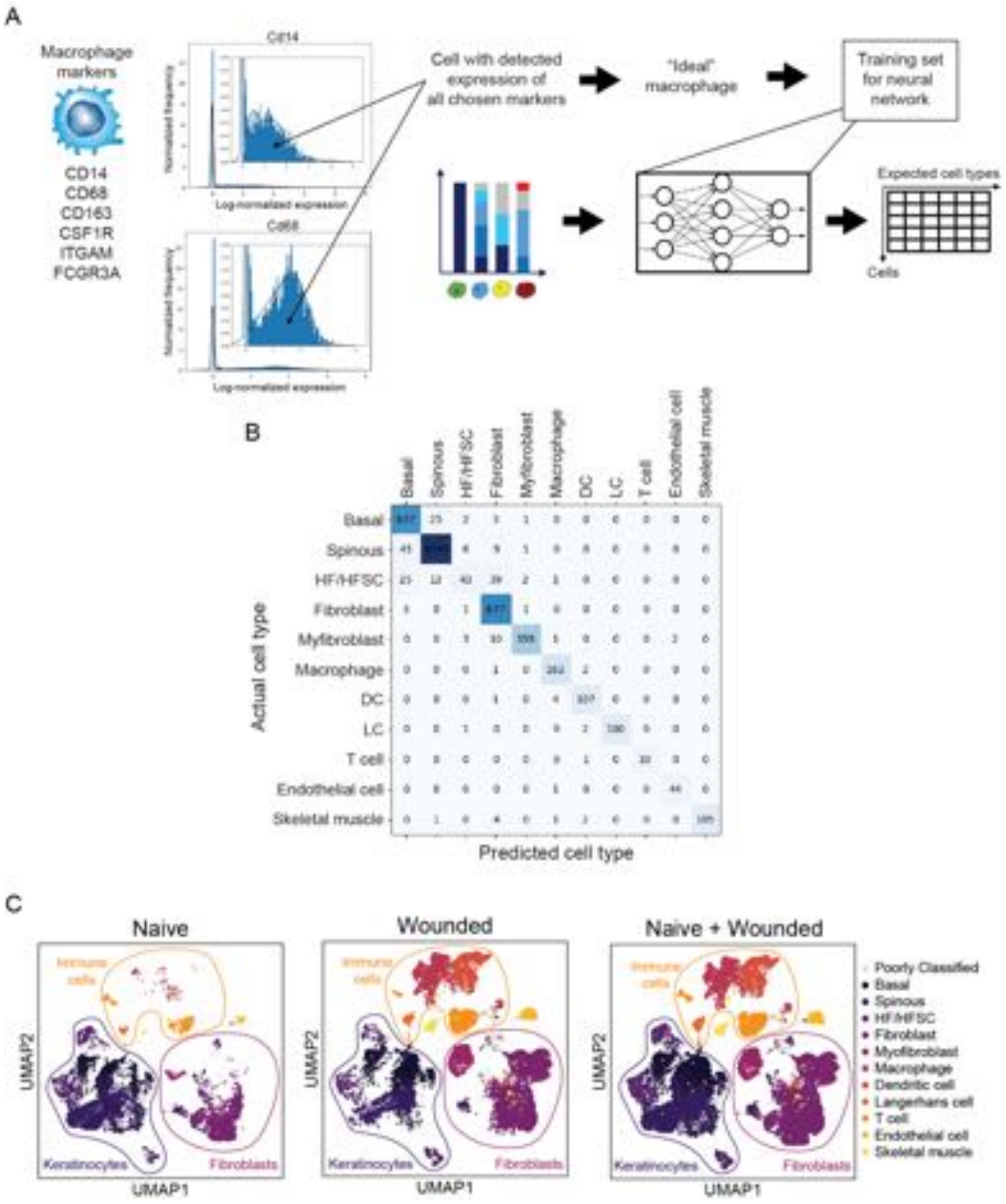

Figure 2: Identification of skin cell types in single-cell RNA sequencing data. (A) Schematic depicting neural network training for cell type identification, using macrophages as an example. In summary, canonical marker genes for a macrophage are defined, cells with detected expression of all chosen markers are defined as “ideal” macrophages, a training set for the neural network is created using “ideal” examples of each cell type, and then neural network scores each cell based on its gene expression and assigns a cell identity. (B) Cell type prediction scores from neural network analysis of GSE142471. (C) Uniform Manifold Approximation and Projection (UMAP) plots of scRNA-seq data (Haensel et al.

(GSE142471)) from mouse skin: non-wounded (Naive), 4-day Wounded, and combined.

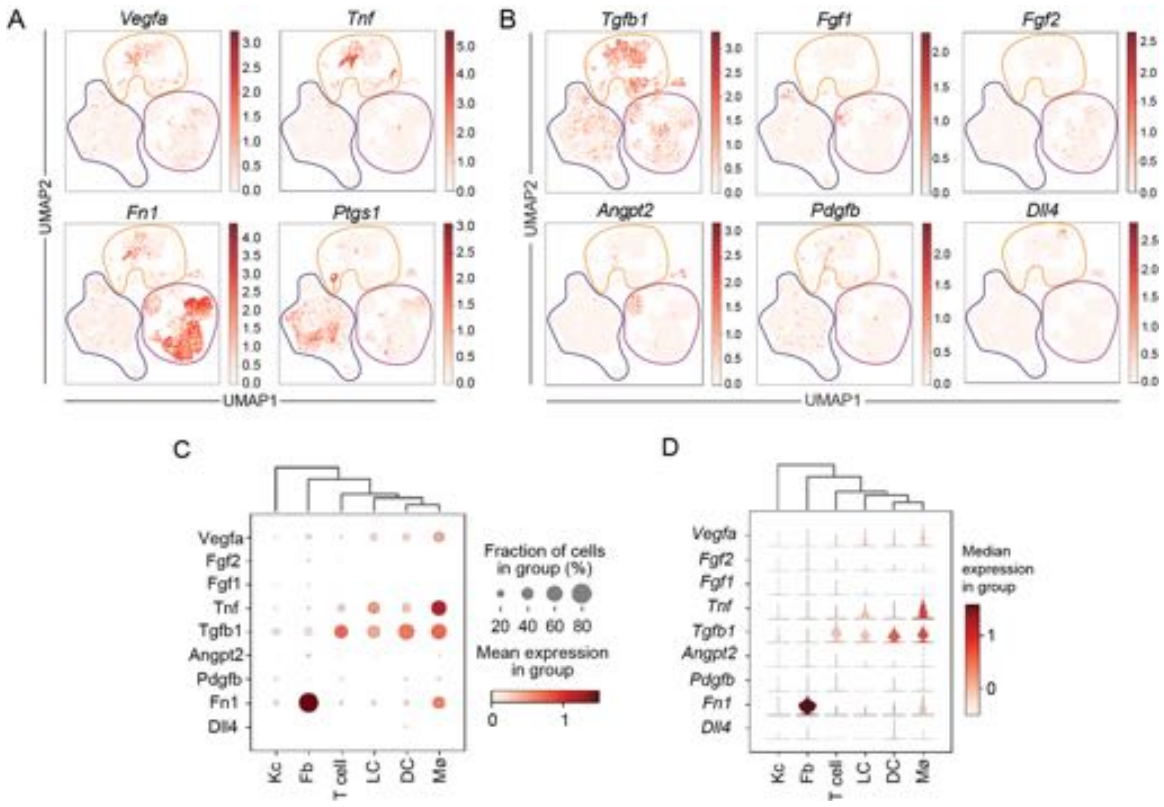

Figure 3: Expression of well-characterized angiogenic ligands in skin cell types. (A) Feature plots showing expression of *Vegfa, Tnf, Ptgs1,* and *Fn1* in single cells of Naive and Wounded skin from Fig. 2C. (B) Feature plots showing expression of established angiogenic genes (*Tgfb1, Fgf1, Fgf2, Angpt2, Pdgfb,* and *Dll4*) in single cells of Naive and Wounded skin from Fig. 2C. (C) Bubble plot depicting average mRNA expression (color) of angiogenic signaling factors expressed by single keratinocytes (Kc), Fibroblasts (Fb), T cells, Langerhans cells, Dendritic cells (DC), and Macrophages (Mø) in wounded and nonwounded samples from Fig. 2C. Bubble size indicates the percent of cells expressing that gene. (D) Violin plots depicting median gene expression of established angiogenic genes in keratinocytes (Kc; includes basal, spinous, and HF/HFSC keratinocytes), fibroblasts (Fb; includes myofibroblasts and fibroblasts) T cells, Langerhans cells (LC), dendritic cells (DC), and macrophages (Mø).

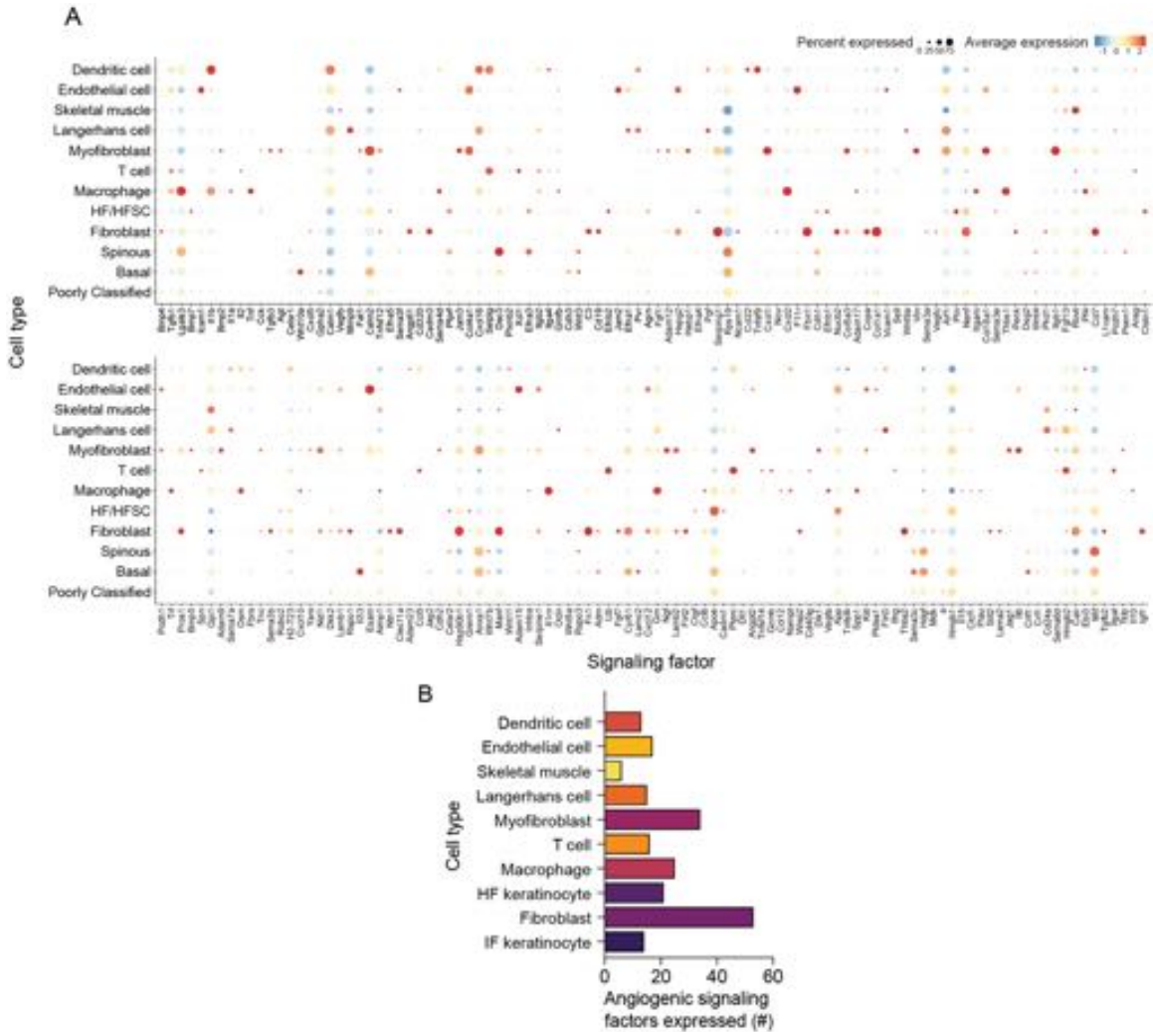

Figure 4: Expression of inferred angiogenic ligands across skin cell types. (A) Bubble plot depicting average mRNA expression (color) of angiogenic signaling factors expressed by different cell types in wounded and nonwounded samples from GSE142471. Signaling factors include the 202 genes identified by NicheNet as potential regulators of the wound-induced gene expression changes in endothelial cells. Bubble size indicates the percent of cells expressing that gene. (B) Quantification of the number of angiogenic signaling factors with an average mRNA expression level ≥1 in each indicated cell type.

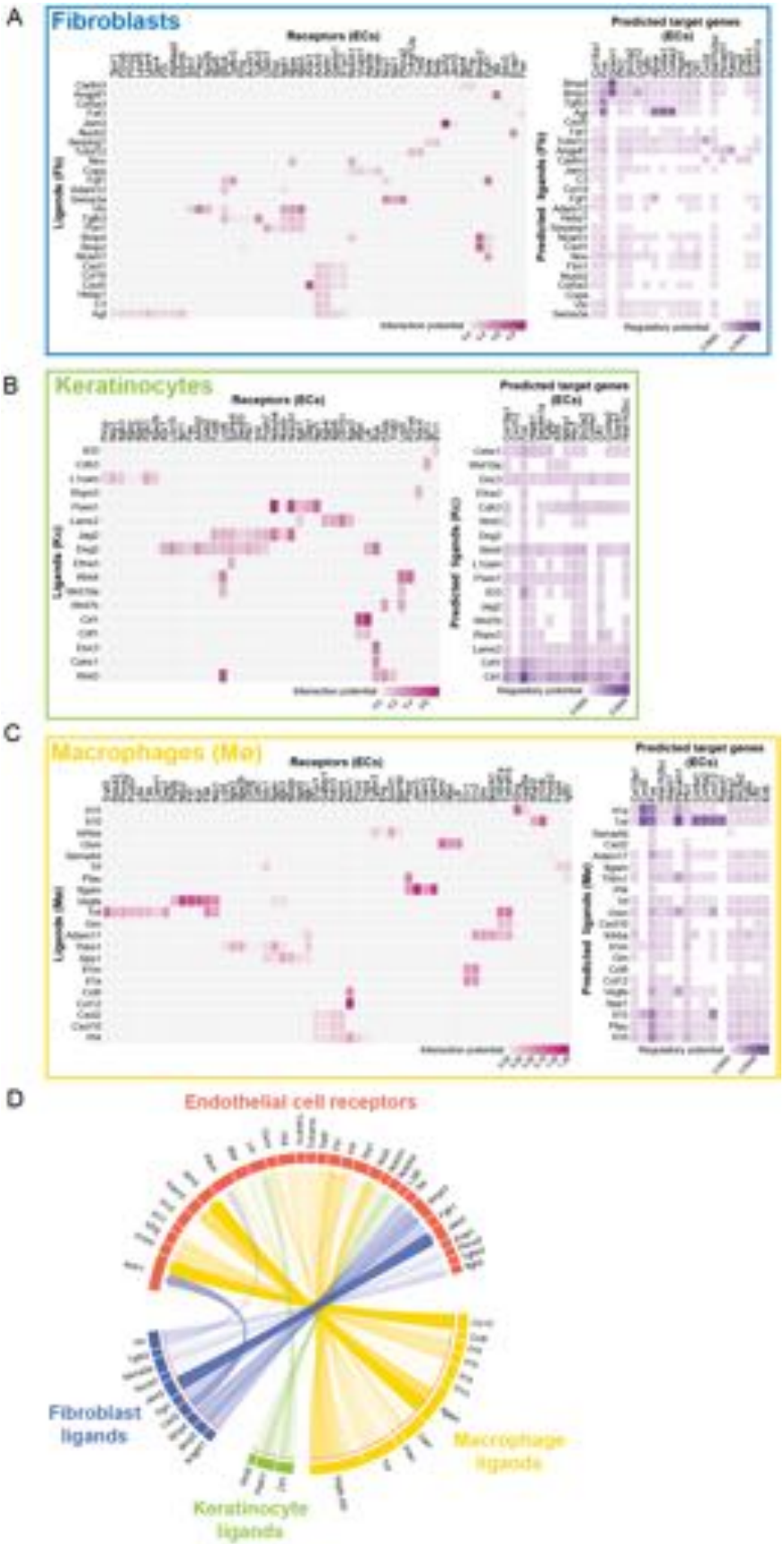
A
Fibroblasts
Receptors (ECs)
Predicted target genes (ECs)
Ligands (Fb)
Predicted ligands (Fb)
B
Keratinocytes
Receptors (ECs)
Predicted target genes (ECs)
Ligands (Ke)
Predicted ligands (Ke)
C
Macrophages (Mø)
Receptors (ECs)
Predicted target genes (ECs)
Ligands (Mø)
Predicted ligands (Mø)
D
Endothelial cell receptors
Fibroblast ligands
Macrophage ligands
Keratinocyte ligands

Figure 5: NicheNet predictions of angiogenic signals in established angiogenic cell types. (A-C) Heatmaps showing potential links between ligands expressed by Fb (A), Kc (B), and Mø (C) and receptors expressed by endothelial cells (ECs) (left) and between Fb (A), Kc (B), and Mø (C) ligands and EC downstream target genes (right). Fibroblast data includes fibroblast and myofibroblast populations. Keratinocyte data includes basal, spinous, and HF/HFSC populations. (D) Chord diagram summarizing the top 50 ligand-receptor links.

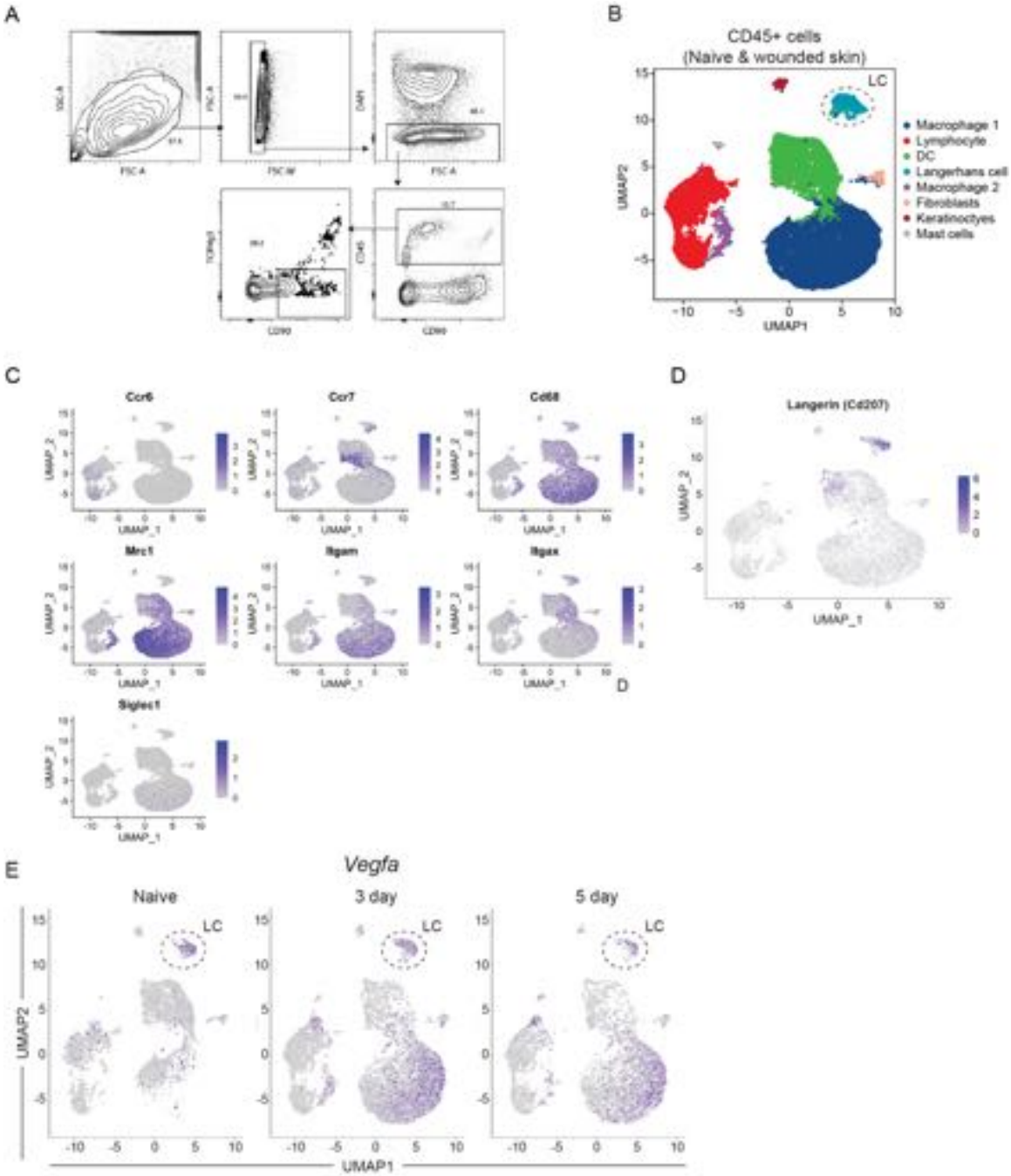

Figure 6: scRNA-sequencing reveals that LCs express Vegfa in naive and wounded skin. (A) FACS sorting scheme to enrich for immune cells for scRNA-seq analysis in GSE166950. (B) UMAP plot of scRNA-seq data of FACS-purified CD45+ cells from nonwounded and wounded (3-day and 5-day post-injury) (GSE166950). Dashed circle identifies Langerhans cell (LC) cluster. (C) Feature plots showing expression of established immune cell markers for GSE166950. (D) Feature plot showing Cd207 (langerin) expression for GSE166950. Dashed circle highlights the population of langerin+ Langerhans cells. (E) Feature plots showing expression of *Vegfa* mRNA in scRNA-seq samples from non-wounded (Naive) skin, 3-day wounds, and 5-day wounds. Dashed circle highlights LC cluster.

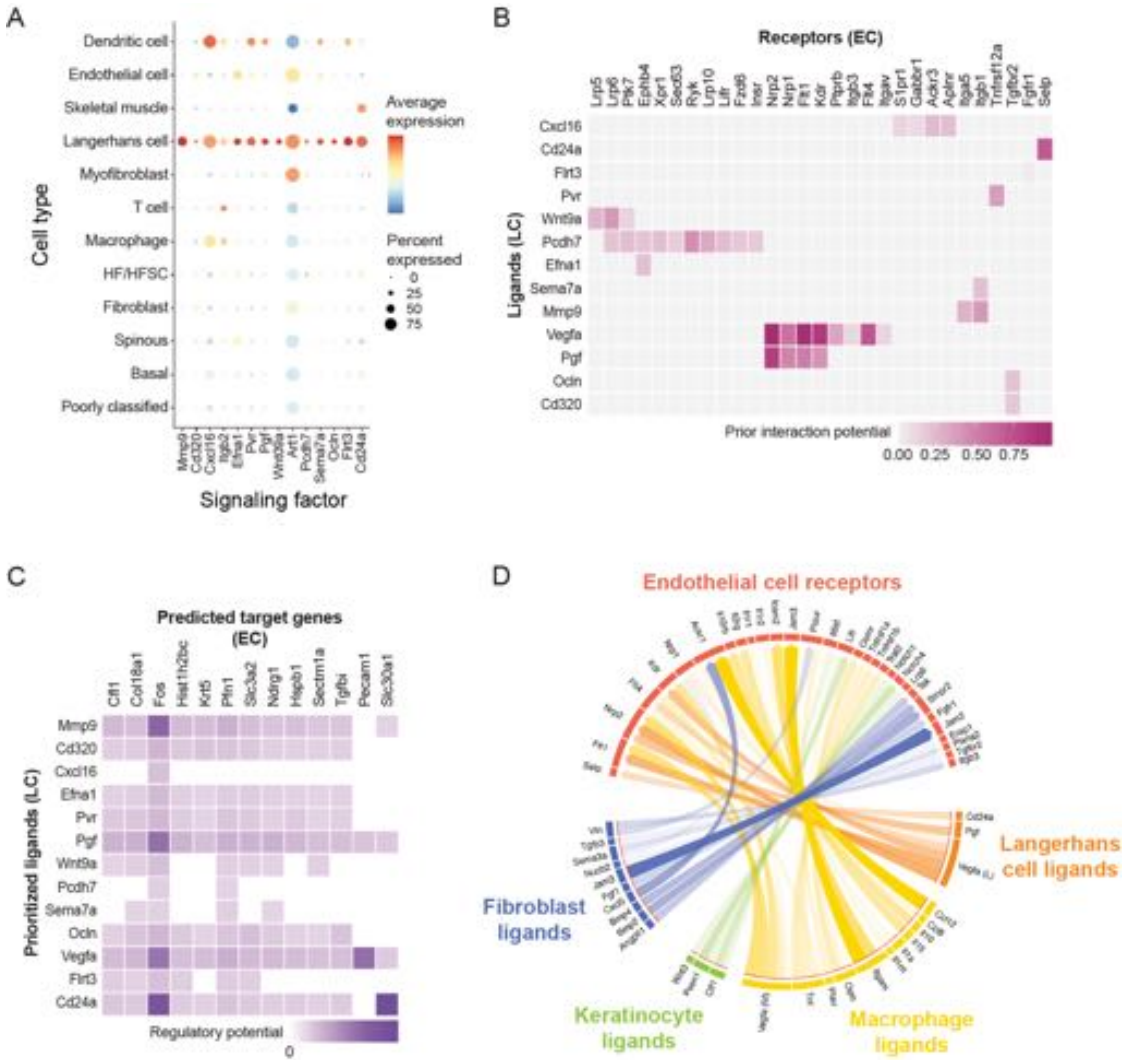

Figure 7: NicheNet predictions reveal that LCs express a unique program of angiogenic signals. (A) Bubble plot depicting average mRNA expression (color) of angiogenic signaling factors expressed by LCs in wounded and nonwounded samples from Haensel et al. (GSE142471). Bubble size indicates the percent of cells expressing that gene. (B) Heatmap showing potential links between ligands expressed by LCs and receptors expressed by endothelial cells (ECs). (C) Heatmap showing potential links between LC ligands and EC downstream target genes. (D) Chord diagram summarizing the top 50 ligand-receptor links during wound healing from GSE142471. Arrows represent ligands from fibroblasts, keratinocytes, macrophages, and Langerhans cells binding to EC receptors.

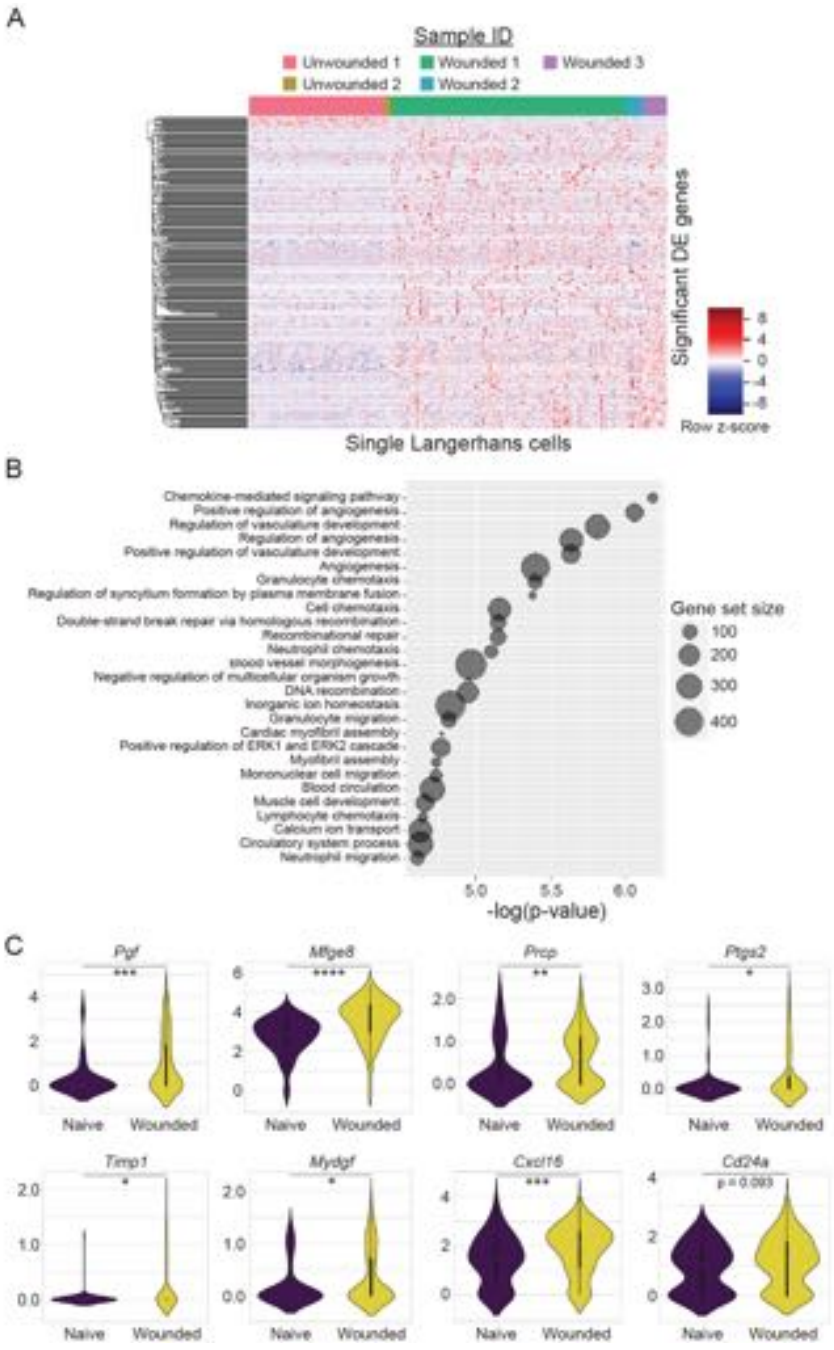

Figure 8: LCs upregulate angiogenic genes in response to injury. (A) Heatmap of differentially expressed genes in LCs from wounded and nonwounded skin. (B) Plot of gene ontology (GO) terms associated with changes in LC gene expression during wound healing. (C) Violin plots of LC mRNA expression of *Pgf, Mfge8, Prcp, Ptgs2, Timp1, Mydgf, Cxcl16,* and *Cd24a* transcripts in wounded and nonwounded samples. *p < 0.05, **p < 0.005, ***p < 0.0005, ****p < 0.00005.

Biological function	Genes (p-adj < 0.05, pval < 0.05)
Chemokine-mediated signaling pathway	***Cxcl2, Ccl2, Cxcl1,*** *Cxcl10, Ccr1, Cxcl5, Hif1a, Ccl8, Ackr3, Gpr35, Ccl3, Slit3, Ccl7*
Positive regulation of angiogenesis	***Pkm, Pgf, Mydgf,*** *Sp1,* ***Hspb1, Lgals3, Ninj1,*** *Pdcl3, Serpine1,* ***Il1b,*** *Hif1a, Vegfa, Tjp1, Btg1, Pdcd6, Vegfb, F3, Tgfbr2, Hmgb1, Aggf1, Xbp1, Cd40, Runx1, Nrp1, Il10, Anxa3, Stat3, Thbs1, Sfrp2, Itga5, Adam12, Zc3h12a, Il10, Anxa3, Stat3, Thbs1, Sfrp2, Itga5, Adam12, Zc3h12a, Itgax*
Regulation of vasculature development	***Pkm, Ccl2, Pgf, Mydgf,*** *Sp1,* ***Hspb1, Lgals3, Ninj1,*** *Pdcl3,* ***Efna1,*** *Cxcl10, Serpine1,* ***Il1b,*** *Hif1a, Spred1, Sars, Vegfa, Tjp1, Btg1, Pdcd6, Gpr4, Vegfb, F3, Tgfbr2, Efna3, Hmgb1, Aggf1, Xbp1, Cd40, Runx1, Plk2, Stat1, Rnh1, Nrp1, Plxnd1, Emp2, Il10, Anxa3, Foxj2, Stat3, Thbs1, Foxo4, Sfrp2, Itga5, Col4a2, Adam12, Zc3h12a, Itgax*
Regulation of angiogenesis	***Pkm, Ccl2, Pgf, Mydgf,*** *Sp1,* ***Hspb1, Lgals3, Ninj1,*** *Pdcl3,* ***Efna1,*** *Cxcl10, Serpine1,* ***Il1b,*** *Hif1a, Spred1, Sars, Vegfa, Tjp1, Btg1, Pdcd6, Gpr4, Vegfb, F3, Tgfbr2, Efna3, Hmgb1, Aggf1, Xbp1, Cd40, Runx1, Plk2, Stat1, Rnh1, Nrp1, Plxnd1, Emp2, Il10, Anxa3, Foxj2, Stat3, Thbs1, Foxo4, Sfrp2, Itga5, Col4a2, Adam12, Zc3h12a, Itgax*
Positive regulation of vasculature development	***Pkm, Pgf, Mydgf,*** *Sp1,* ***Hspb1, Lgals3, Ninj1,*** *Pdcl3, Serpine1,* ***Il1b,*** *Hif1a, Vegfa, Tjp1, Btg1, Pdcd6, Vegfb, F3, Tgfbr2, Hmgb1, Aggf1, Xbp1, Cd40, Runx1, Nrp1, Il10, Anxa3, Stat3, Thbs1, Sfrp2, Itga5, Adam12, Zc3h12a, Itgax*
Angiogenesis	***Mfge8, Pkm, Ccl2, Anxa1, Pgf, Stk4,*** *Cdc42,* ***Prcp, Adipor2, Atp5b, Mydgf,*** *Sp1,* ***Hspb1, Lgals3, Ptgs2, Ninj1, Rbpj,*** *Pdcl3,* ***Efna1, Tnfaip2, Actg1,*** *Nfatc3, Fn1, Bcas3, Cxcl10, Plau, Serpine1,* ***Il1b,*** *Hif1a, Spred1, Sars, Vegfa, Tjp1, Tgfbr1, Btg1, Efnb2, Pdcd6, Gpr4, Vegfb, F3, Tgfbr2, Anxa2, Efna3, Mmp19, Ackr3, Hmgb1, Aggf1, Xbp1, Cd40, Plcd1, Apold1, Runx1, Plk2, Adam8, Stat1, Rnh1, Nrp1, Plxnd1, Emp2, B4galt1, Il10, Anxa3, Col4a1, Foxj2, Clic4, Stat3, Thbs1, Pdcd10, Foxo4, Sfrp2, Itga5, Col4a2, Lemd3, Adam12, Nus1, Zc3h12a, Itgax*
Granulocyte chemotaxis	***Csf1r, Cxcl2, Ccl2, Anxa1, S100a8, Cxcl1, Ppia, Prex1, Lgals3, Ppib,*** *Pde4d, Nckap1l, Cxcl10, Cxcl5, Il1b, S100a9, Vegfa, Nod2, Ccl8, Pde4b, C1qbp, Cklf, Rac1, Slamf1, Thbs4, Vav1, Ccl3, Mapk1, Thbs1, Il23a, Ccl7*

Table 1: Angiogenic genes differentially expressed in LCs after injury. Bolded genes have a p-adj value < 0.05. Non-bolded genes have a p-value < 0.05.

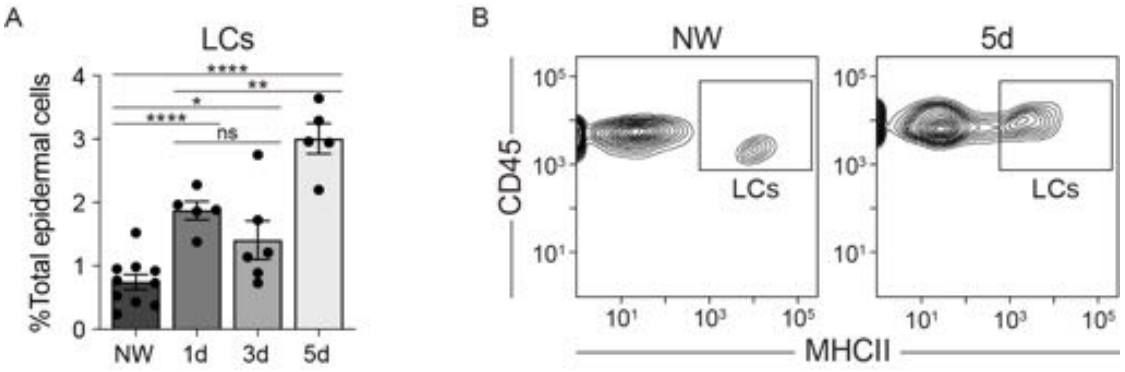

Figure 9: Flow cytometry quantification of LCs in the epidermal edges of wounds. (A) Flow cytometry quantification of LCs in nonwounded (NW) epidermis and epidermal edges of WT skin wounds 1, 3, and 5 days after injury. LCs quantified as a percent of total epidermal cells Data are 5-9 mice as indicated. Error bars indicate mean +/- SEM. *p < 0.05, **p < 0.005, ***p < 0.0005, ****p < 0.00005. (B) Representative flow cytometry plots of LCs (CD45+ MHCII+ epidermal cells) in nonwounded epidermis (NW, left) and at the edges of 5-day wounds (5d, right) in WT mice.

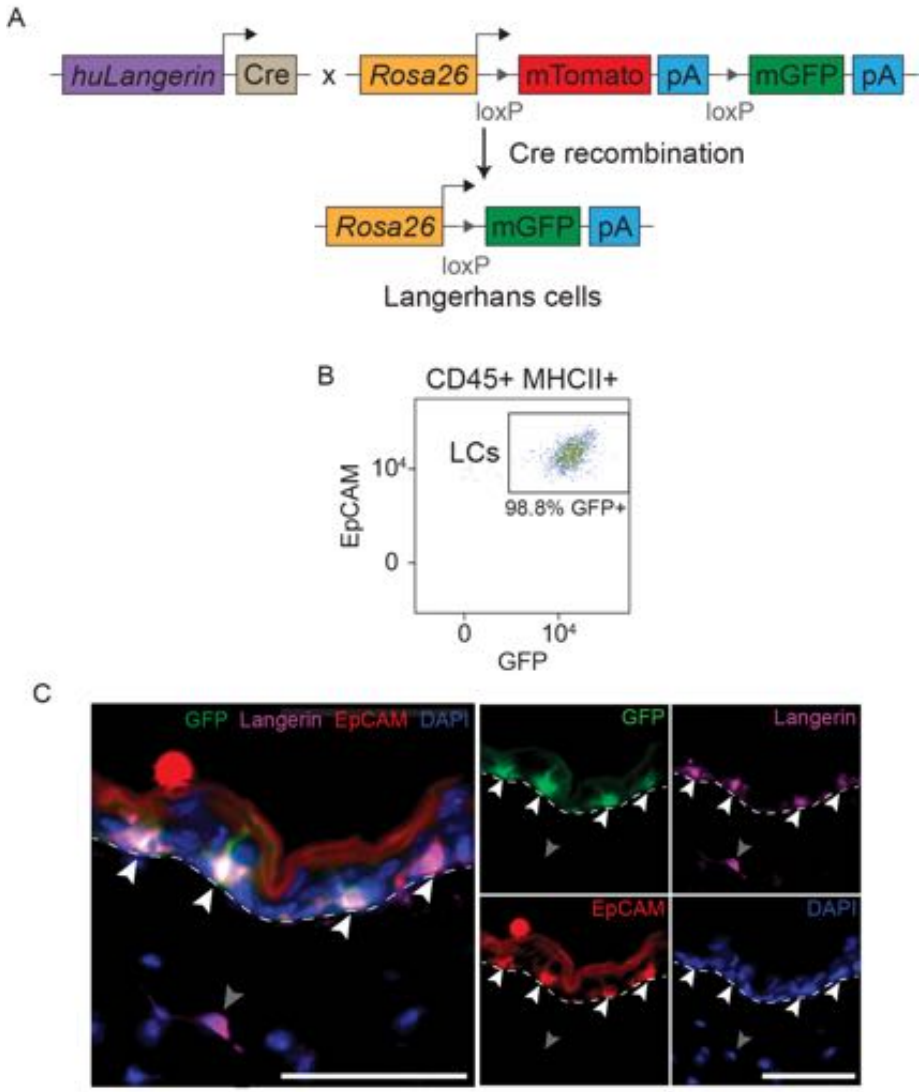

Figure 10: LCs are efficiently and specifically labeled in LC-iGFP reporter mice. (A) Schematic summarizing genetic strategy to express membrane-associated GFP (mGFP) in mature LCs in *huLang*-CreER/mTmG (LC-iGFP) inducible fluorescent reporter mice. (B) Representative flow cytometry plot demonstrating the efficiency of GFP labeling of mature LCs (CD45+ MHCII+ epidermal cells) in LC-iGFP mice. (C) Fluorescence imaging of GFP+ LCs (green), langerin (magenta), EpCAM (red), and DAPI (blue) in cross-sections of naive skin from LC-iGFP mice. White arrows label GFP+, EpCAM+, langerin+ LCs. Gray arrows label GFP- EpCAM- langerin+ dermal DCs. White dashed line outlines the epidermis. Scale bars, 100 μm.

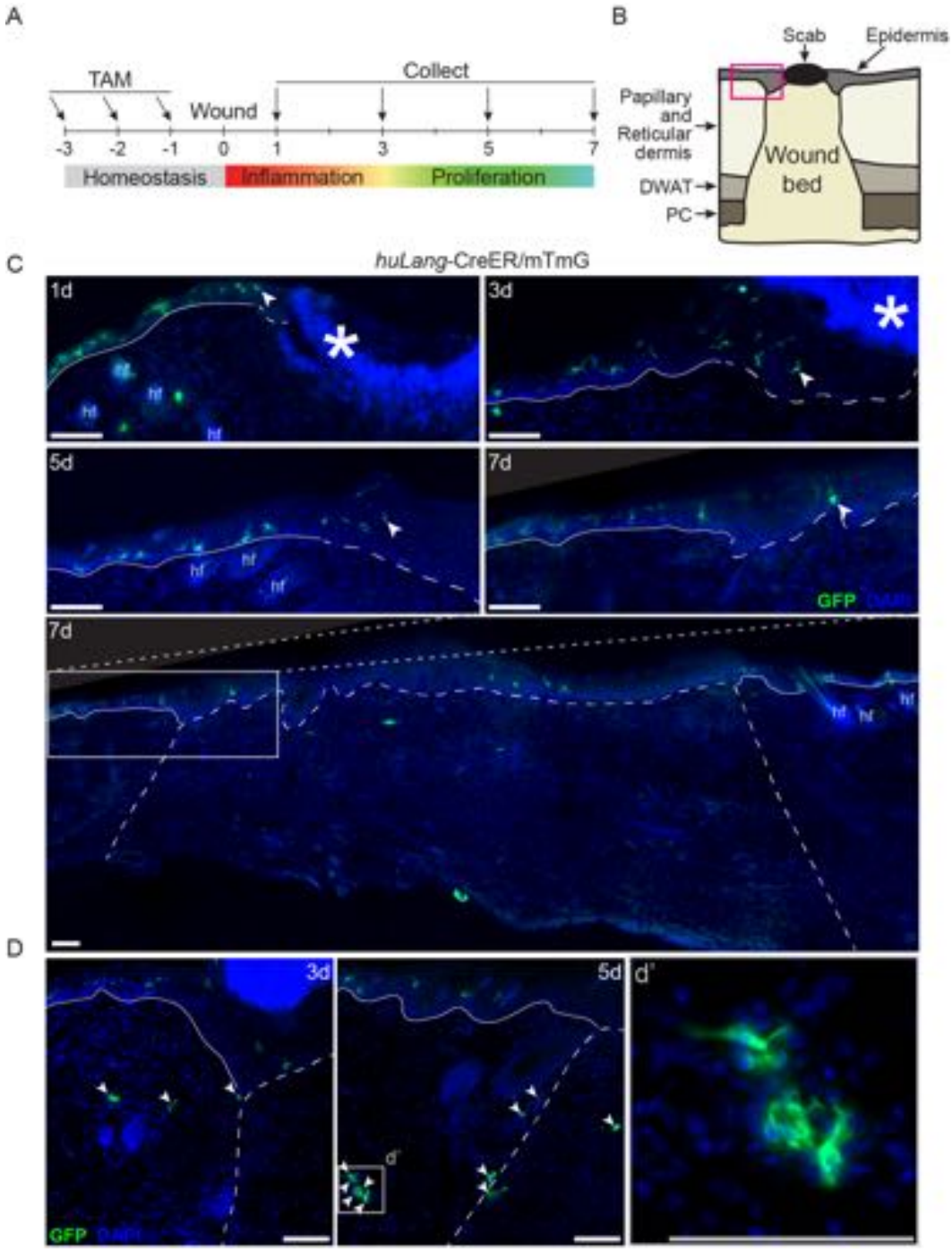

Figure 11: LCs are present at the epidermal and dermal edges of skin wounds. (A) Schematic depicting tamoxifen treatment timeline and wound healing time points for histological analysis of LC-iGFP mice. (B) Schematic of skin wound cross-section. Pink box outlines the epidermal wound edge. DWAT = dermal white adipose tissue, PC = panniculus carnosus. (C) Fluorescent imaging of GFP+ LCs (green) and DAPI (blue) in epidermal wound edges 1, 3, 5, and 7 days after injury in LC-iGFP mice. Solid white lines trace the non-wounded epidermis, and the dashed white lines delineate the wound bed. White arrows label the LC closest to

the wound center. Asterisks indicate non-specific labeling of scab, hair follicles (hf). Scale bars, 100 μm. (D) Fluorescent imaging of GFP+ LCs in the dermis at wound edges of 3- and 5-day wounds. White arrows label LCs in dermis and wound bed. White dashed lines delineate wound edges. Scale bars, 100 μm.

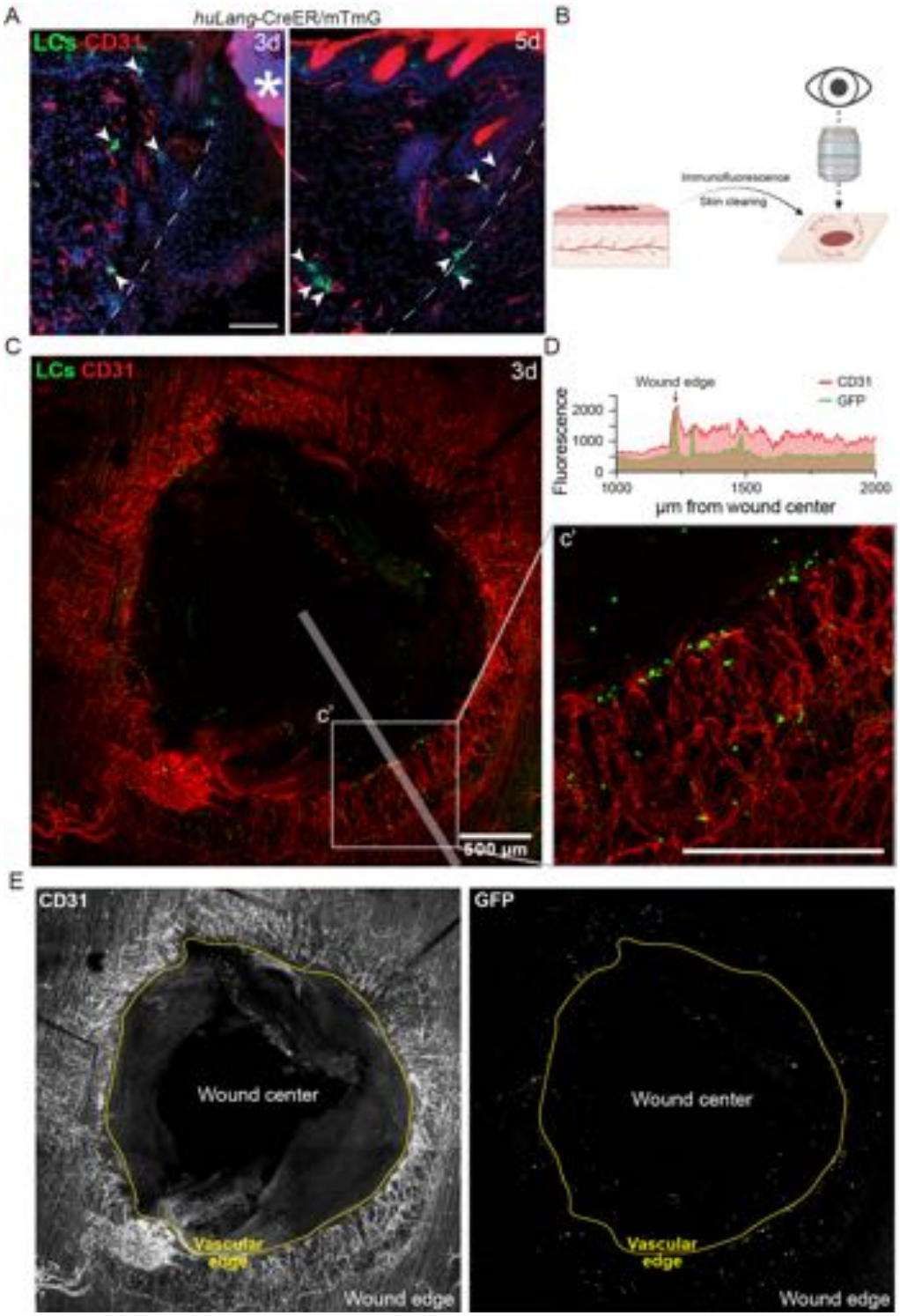

Figure 12: LCs localize near blood vessels in skin wounds. (A) Imaging of GFP+ LCs (green) and immunostaining of CD31+ blood vessels (red) in cross-sections of 3- and 5-day wounds from LC-iGFP mice. Arrows label LCs close to blood vessels. White dashed lines delineate wound edges. Asterisks (*) indicates non-specific labeling of scab. Scale bars, 100 µm. (B) Schematic depicting the

orientation of 3-dimensional wound beds for whole mount confocal microscopy. (C) Maximum intensity projection of confocal imaging of CD31+ blood vessels (red) and GFP+ LCs (green) in 3-day whole mount wounds of LC-iGFP mice. Transparent white line depicts line scan path quantified in D. Scale bar, 500 μm. (D) Quantification of CD31 (red) and GFP (green) fluorescence in line scan (75 μm wide) along wound radius. Arrow indicates wound edge. (E) Maximum intensity projections of confocal imaging of CD31+ blood vessels (left) and GFP+ LCs (right) in 3-day whole mount wounds of LC-iGFP mice. Yellow line outlines the vascular edge of the wound.

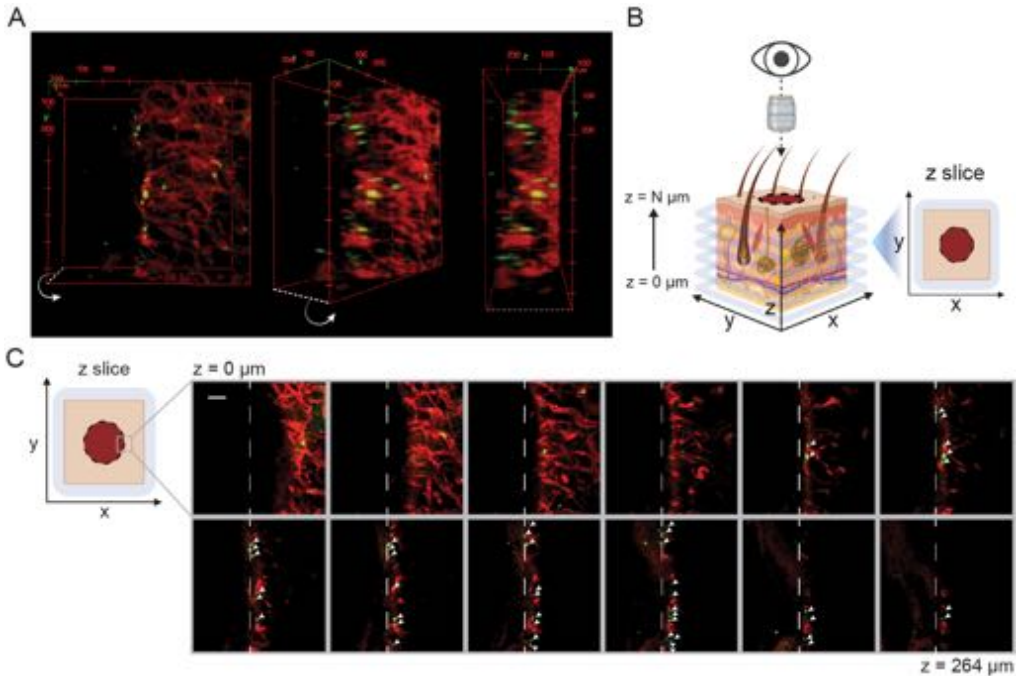

Figure 13: Wound-edge LCs localize near the tips of blood vessels. (A) 3-Dimensional volume rendering of CD31+ blood vessels (red) and GFP+ LCs (green) at the edges of a 3-day wound in a LC-iGFP mouse. (B) Schematic depicting the orientation of optical z-slices acquired from confocal microscopy of whole mount wound beds. (C) Montage of z-slice images from deep (z = 0 µm) to superficial (z = 264 µm) depth of a 3-day LC-iGFP wound bed. White arrows indicate GFP+ LCs (green) close to CD31+ (red) blood vessels at the wound leading edge (white dashed lines). Scale bar, 100 µm.

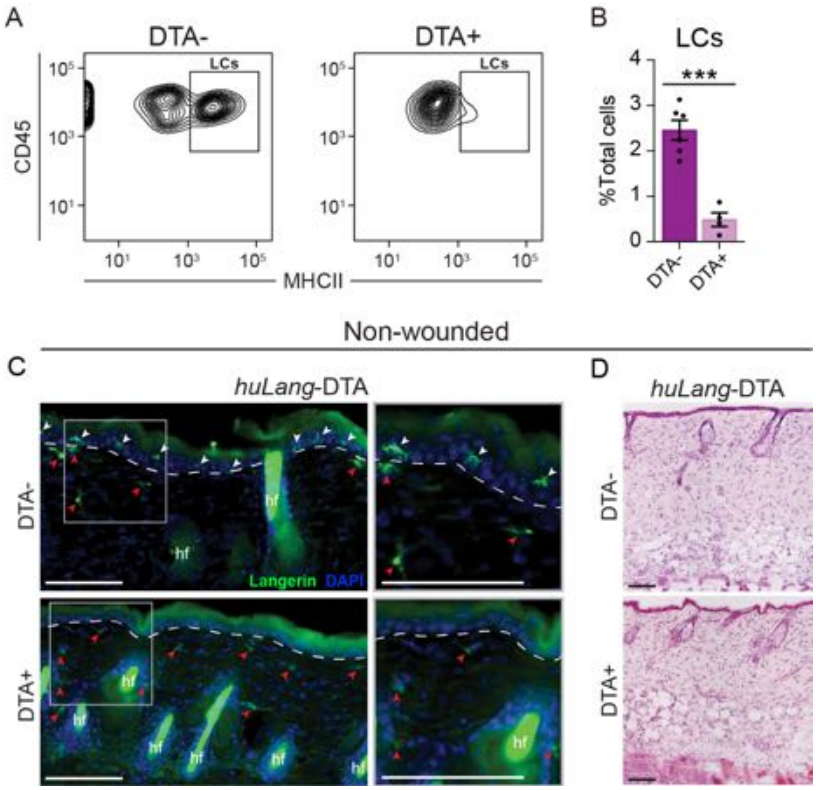

Figure 14: Characterization of LC depletion and skin morphology in *huLang*-DTA mice. (A-B) Flow cytometry plots (A) and quantification (B) of LCs (CD45+ MHCII+ epidermal cells) from wound-edge epidermal preps in *huLang*-DTA+ mice and DTA- littermate controls. Data are 3-5 mice. Error bars indicate mean +/- SEM. ***p < 0.0005.

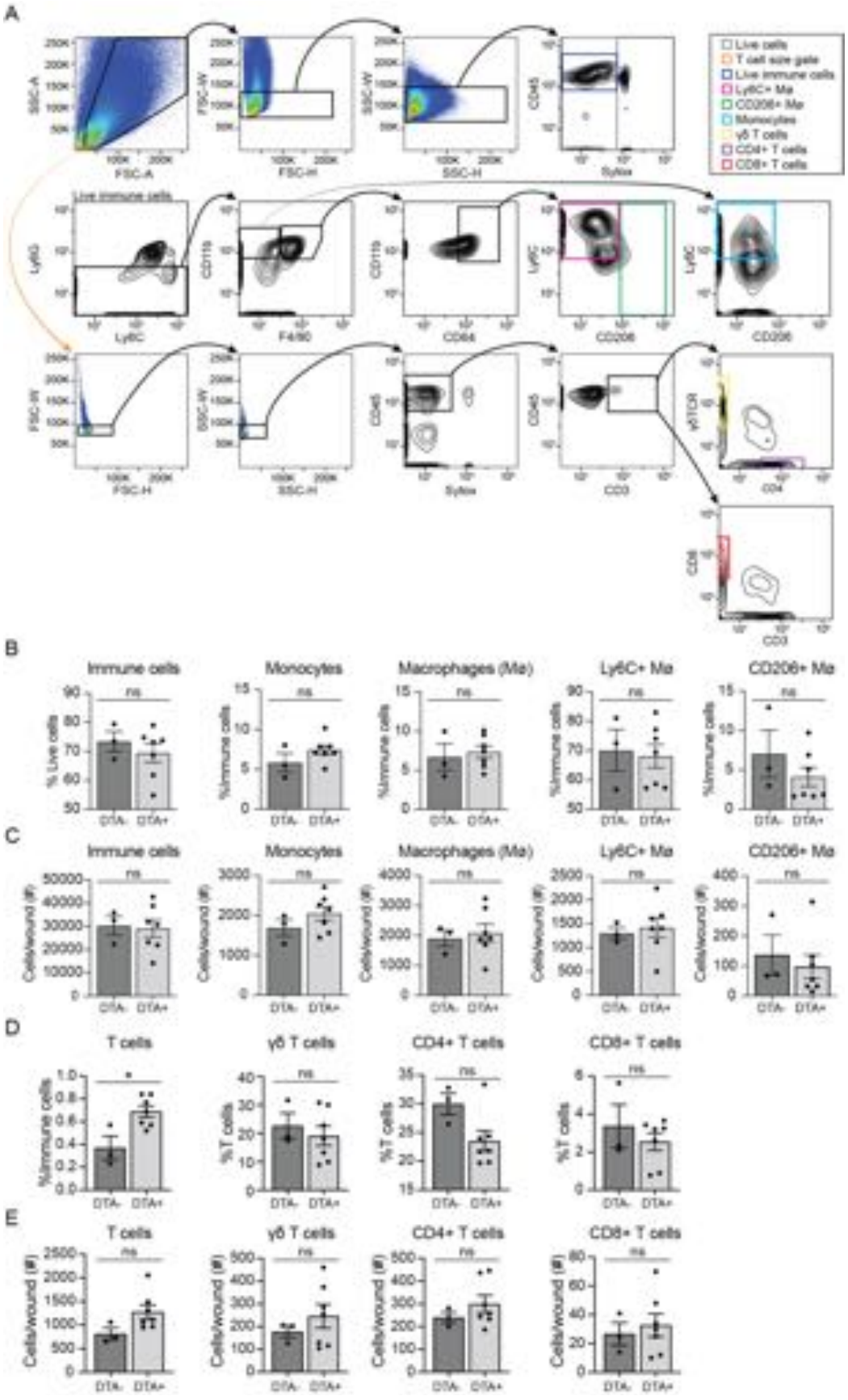
A
Live cells
T cell size gate
Live immune cells
Ly6C+ Mø
CD206+ Mø
Monocytes
γδ T cells
CD4+ T cells
CD8+ T cells
Live immune cells
B
Immune cells
Monocytes
Macrophages (Mø)
Ly6C+ Mø
CD206+ Mø
% Live cells
%Immune cells
ns
DTA-
DTA+
C
Immune cells
Monocytes
Macrophages (Mø)
Ly6C+ Mø
CD206+ Mø
Cells/wound (#)
ns
DTA-
DTA+
D
T cells
γδ T cells
CD4+ T cells
CD8+ T cells
%Immune cells
%T cells
*
ns
DTA-
DTA+
E
T cells
γδ T cells
CD4+ T cells
CD8+ T cells
Cells/wound (#)
ns
DTA-
DTA+

Figure 15: Immune cell recruitment in huLang-DTA mice 3 days after injury is normal. (A) Plots depicting the flow cytometry gating strategy to identify and quantify multiple immune cell types: Live cells (Sytox-; gray box), T cell size gate (orange), Live immune cells (CD45+ Sytox-; navy), Ly6C+ macrophages (Mø) (CD45+ Ly6G- CD11b+ F4/80+ CD64+ Ly6C+; pink), CD206+ Mø (CD45+ Ly6G- CD11b+ F4/80+ CD64+ CD206+; green), monocytes (CD45+ Ly6G- CD11b+ F4/80- Ly6C+; light blue), γδ T cells (CD45+, CD3+, γδTCR+; yellow), CD4 T cells (CD45+, CD3+, CD4+; purple), and CD8 T cells (CD45+, CD3+, CD8+; red). (B-C) Relative quantification (B) and absolute counts (C) of myeloid cell types (monocytes and macrophages) in 3-day wounds from *huLang*-DTA+ mice and DTA- littermate controls. Data are 3-7 mice. Error bars indicate mean +/- SEM. ns, no statistical significance. (D-E) Relative quantification (D) and absolute counts (E) of T cell populations in 3-day wounds from *huLang*-DTA+ mice and DTA- littermate controls. Data are 3-7 mice. Error bars indicate mean +/- SEM. *$p < 0.05$. ns, no statistical significance.

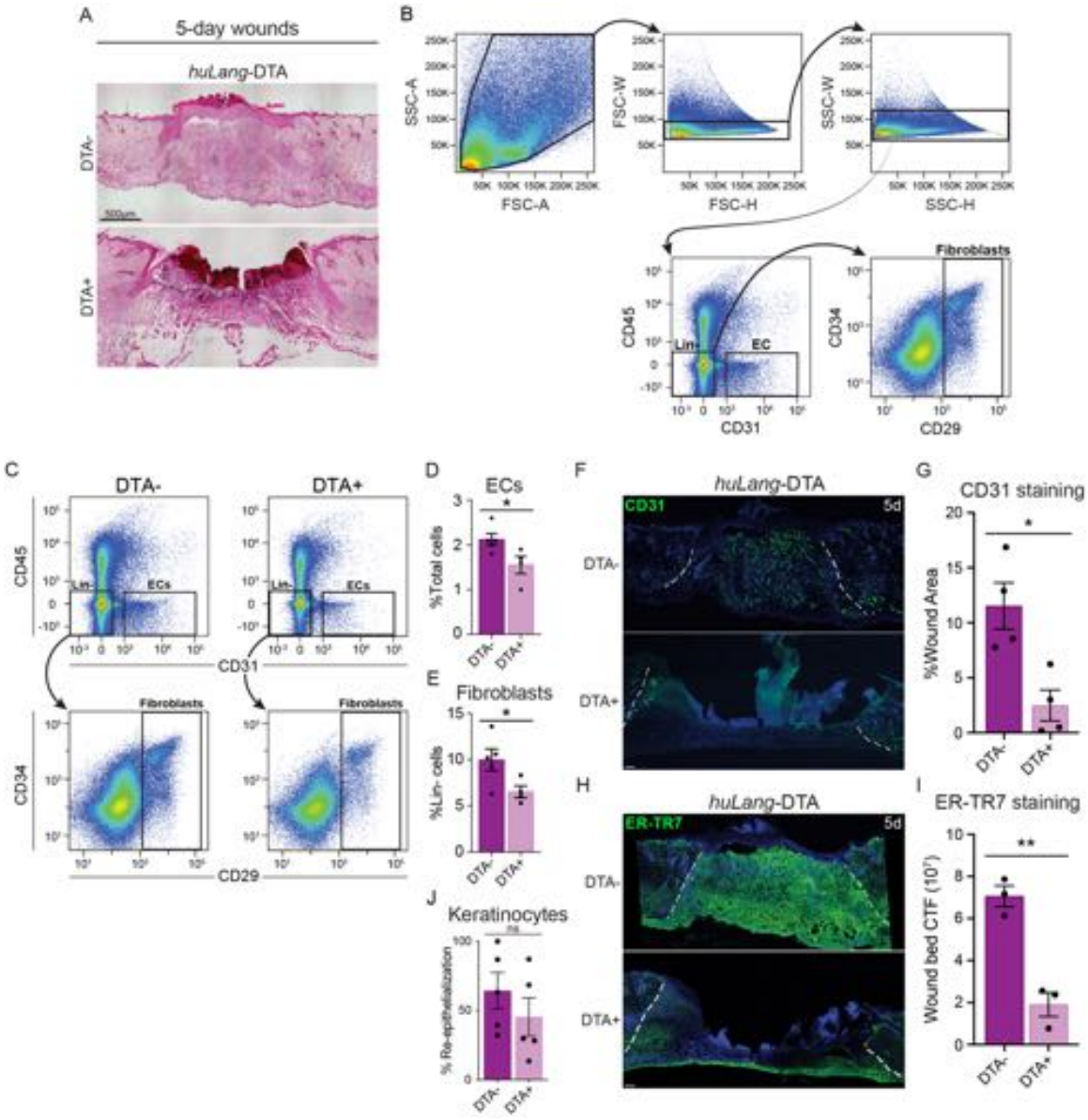

Figure 16: Multiple facets of skin repair are defective in *huLang*-DTA mice. (A) H&E staining of 5-day wounds from *huLang*-DTA+ mice and controls. Scale bars, 500 μm. (B) Plots depicting the flow cytometry gating strategy to identify lineage-negative cells (Lin-) (CD45- CD31-), endothelial cells (EC) (CD31+ CD45-), and fibroblasts (Lin- CD29+). (C-D) Flow cytometry plots (C) and quantification of endothelial cells (ECs; CD31+ CD45-) (D) and fibroblasts (Fb; lineage (Lin)- CD29+) (E) in 5-day wound beds from *huLang*-DTA+ mice and DTA- littermate controls. Data are 3-5 mice. Error bars indicate mean +/- SEM. ***$p < 0.0005$. *$p < 0.05$. (F-G) Images (F) and quantification (G) of CD31 immunostaining (green) and DAPI (blue) in cross-sections of 5-day wound beds from *huLang*-DTA and control mice. White dashed lines delineate wound edges. Scale bars, 100 μm. Data are 4 mice. Error bars indicate mean +/- SEM. *$p < 0.05$. (H-I) Images (H) and quantification (I) of ER-TR7 immunostaining to label fibroblasts (green) in

cross-sections of 5-day wound beds from *huLang*-DTA and control mice. White dashed lines delineate the wound edges. Scale bars, 100 μm. Data are 3 mice. **p < 0.005. (J) Quantification of re-epithelialization as measured by percent of wound bed covered with DAPI+ epithelium in 5-day wounds from *huLang*-DTA+ mice and controls. Data are 5 mice. Error bars indicate mean +/- SEM. ns, no statistical significance.

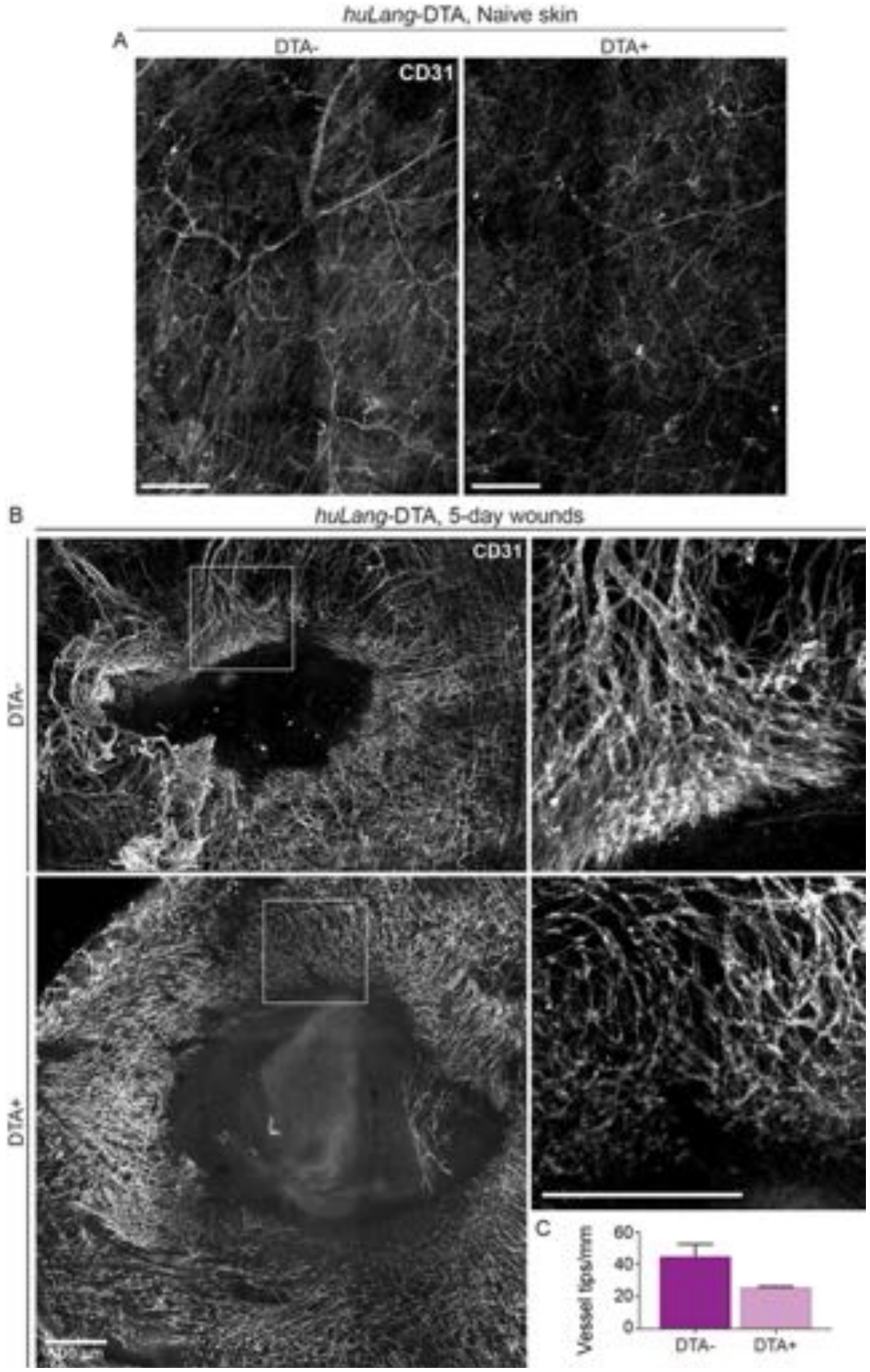
huLang-DTA, Naive skin
A
DTA-
DTA+
CD31
B
huLang-DTA, 5-day wounds
CD31
DTA-
DTA+
C
Vessel tips/mm
60
40
20
0
DTA-
DTA+

Figure 17: Blood vessel morphology is defective in *huLang*-DTA mice. (A) Maximum intensity projections of confocal imaging of CD31+ blood vessels (white) in whole mounts of naive skin from *huLang*-DTA mice. Scale bars, 500μm. (B) Maximum intensity projections of confocal imaging of CD31+ blood vessels (white) in whole mounts of 5-day wound beds from *huLang*-DTA mice. Insets provide higher magnification view of branching vessels at wound edges. Scale bars, 500μm. (C) Quantification of the number of blood vessel tips per mm wound edge in 5-day wounds from *huLang*-DTA mice. Data are 2 mice.

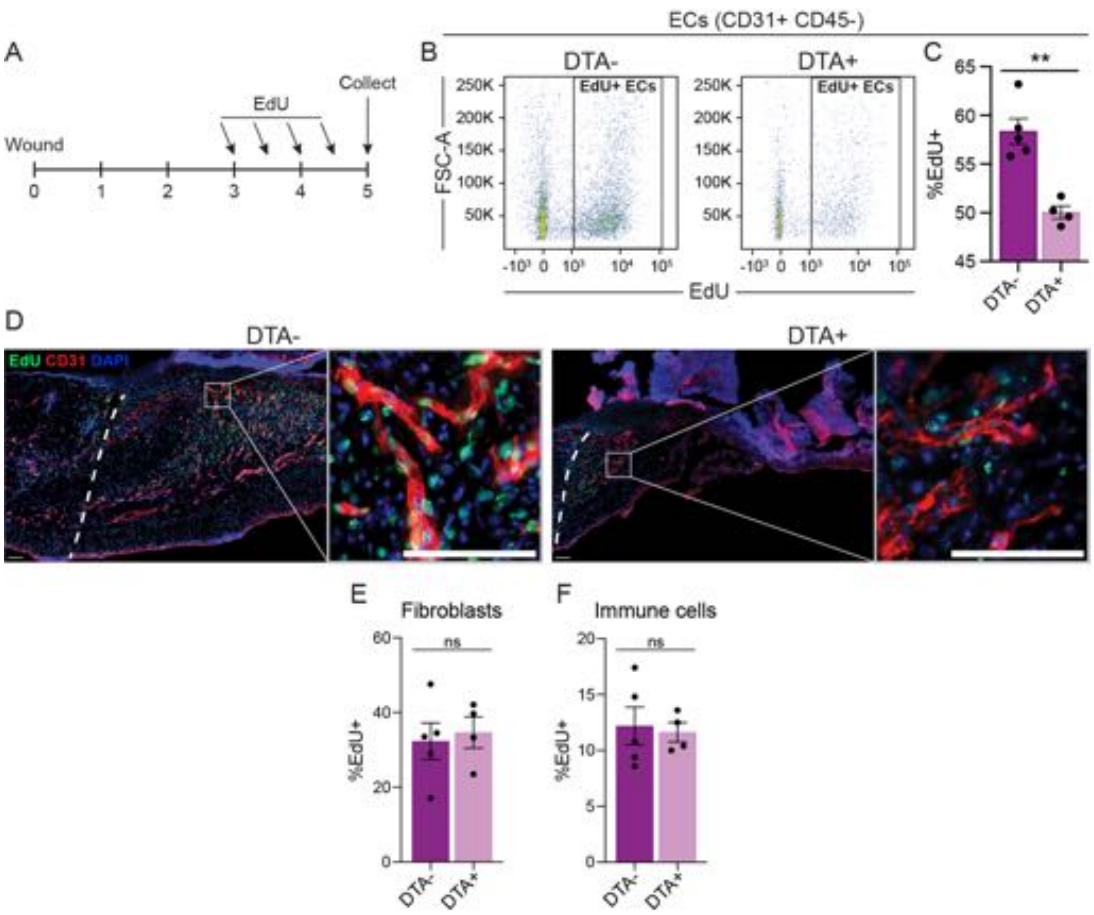

Figure 18: Endothelial cells proliferation is reduced in huLang-DTA mice. (A) Schematic depicting experimental design of EdU pulse-chase experiment in *huLang*-DTA mice and control mice. (B-C) Representative flow cytometry plots (B) and quantification (C) of EdU+ labeling in endothelial cells (ECs; CD31+ CD45- cells) from 5-day *huLang*-DTA wounds. Data are 4-5 mice. Error bars indicate mean +/- SEM. **p < 0.005. (D) Fluorescent imaging of EdU (green) and DAPI (blue) nuclei within CD31+ (red) blood vessels in 5-day wounds of *huLang*-DTA and control (DTA-) mice. (E-F) Quantification of EdU+ fibroblasts (E) and immune cells (F) in 5-day wounds from *huLang*-DTA+ mice and DTA- littermate controls. Data are 4-5 mice. Error bars indicate mean +/- SEM. ns, no statistical significance.

Chapter 5: Summary and perspectives

Our results provide novel insight into the cells and signals that govern the skin's angiogenic niche. Using single-cell mRNA sequencing analyses, we expanded our understanding of how known angiogenic cell types, including fibroblasts, macrophages, and keratinocytes, signal to endothelial cells to induce revascularization. Our transcriptional analyses also revealed that Langerhans cells express a unique angiogenic program, distinct from related cell types such as macrophages, DCs, and keratinocytes. To explore the spatial relationship between LCs and blood vessels, we employed a LC-specific genetic reporter mouse and observed that LCs localize around skin wounds in close proximity to the leading endothelial cell edge, where endothelial tip cells drive blood vessel regrowth. These observations lead us characterize wound healing in LC-depleted mice, which elucidated that LCs are essential for efficient healing. Together, our data contribute to the fields of tissue regeneration, vascular biology, and LC biology.

Langerhans cells contribute to the complex angiogenic niche.

Since angiogenesis is highly relevant to many facets of human health, extensive research has been conducted to characterize the forces and factors that control it (Ucuzian et al., 2010; Potente et al., 2011; Martin and Gurevich, 2021). In these studies, a subset of cells (including macrophages and fibroblasts) and signaling factors (including VEGF, PDGF, FGF, TNF, and Angiopoietins) have received a lot of attention and are regarded as some of the most important angiogenic drivers. VEGF signaling, in particular, is lauded as one of the most

potent and vital angiogenic signaling axes, and was therefore labeled as a highly attractive therapeutic target to stimulate angiogenesis (Shibuya, 2011). However, clinical studies targeting VEGF signaling to promote therapeutic angiogenesis have not been fruitful (Giacca and Zacchigna, 2012; Johnson and Wilgus, 2014), suggesting that inducing revascularization *in vivo* is significantly more complex than agonizing one growth pathway. Our work provides a broad transcriptomic map of angiogenic signaling that occurs in mouse skin wounds, which highlights the breadth of cell types and ligands with the potential to regulate endothelial cell regeneration. Using a sophisticated computational tool, NicheNet, we analyzed scRNA-seq data to (I) identify wound-induced changes in EC gene expression, (II) produce a list of 202 putative ligands with the potential to manipulate the expression of the wound-responsive EC genes, (III) measure the expression of these inferred ligands in each skin cell type, and (IV) calculate scores predicting ligand-receptor binding and subsequent downstream signaling in ECs. With this, we not only validated the expression and regulatory potential of several previously known angiogenic factors (such as *Fgf1* and *Tgfb3* in fibroblasts, and *Vegfa* and *Tnf* in macrophages), but we also highlighted the broader complexity of the angiogenic niche.

When we designed this analysis, we expected to see expression of classical angiogenic factors to be highly enriched in established cell types. Interestingly, the results were not so simple. We were surprised to find that several canonical proangiogenic factors, including *Pdgfb* and *Dll4*, were only modestly expressed across cell types, whereas many of the top predicted ligands expressed fibroblasts,

keratinocytes, and macrophages included genes that are not commonly labeled as proangiogenic factors. This diversity in angiogenic signals further supports the idea that individual signaling factors may be insufficient to drive angiogenesis *in vivo,* and that future clinical trials should explore the effects of combinational therapies toward restoring angiogenesis in chronic wounds (Veith et al., 2019).

Additionally, we were fascinated to see that expression of angiogenic ligands was not restricted to a few specific cell types. Although known proangiogenic cell types, including fibroblasts and macrophages, expressed the highest numbers of angiogenic mRNAs, T cells, DCs, and LCs expressed similar numbers as keratinocytes, which are known to secrete factors that stimulate skin revascularization (Rossiter et al., 2004). Importantly, there was significant heterogeneity in ligands expressed by each cell type, which further highlights the complexity of the niche. Together, this provides rationale to explore the unique contributions of each of these immune cell populations to skin angiogenesis and wound healing.

We took particular interest in LCs and their potential to induce angiogenesis because although they share many similarities to macrophages (Doebel et al., 2017), little was known about their role in tissue repair. Our NicheNet analyses suggested that LCs possess strong angiogenic potential: they express a unique angiogenic program that includes established angiogenic growth factors including *Vegfa* and *Pgf*. Although LC *Vegfa* expression appears modest in our scRNA-seq dataset from all skin cell types, we verified this expression in an additional scRNA-seq dataset in which CD45+ immune cells were enriched. Despite the fact that the

immune-enriched dataset was generated by a different lab using a slightly different wound healing model (described in **Materials & Methods**), the expression of *Vegfa* in LCs is consistent, which speaks to the robustness of this phenotype. Furthermore, in our whole-skin scRNA-seq dataset, we also examined differentially expressed genes between LCs from wounded and nonwounded skin, and found that LCs respond to injury by upregulating their expression of angiogenic genes. Together, these data strongly suggest that LCs are transcriptionally poised to regulate angiogenesis during wound healing, and elucidate several potential molecular mechanisms through which they may be acting.

While our data provide a compelling map of potential LC angiogenic signaling mechanisms, future work is required to validate the presence of these factors at the protein level and to determine what roles they play in skin regeneration *in vivo.* These follow-up experiments are critical for determining the clinical potential of LCs or LC-derived factors. In light of our findings that numerous skin cell types transcribe diverse assortments of angiogenic genes, I predict that cellular therapies, and potentially combinational cellular therapies, will more effectively stimulate *in situ* angiogenesis than will molecular approaches that target one specific signaling axis.

Langerhans cells localize in the wound microenvironment.

After we learned that LCs are transcriptionally poised to promote angiogenesis, we were curious to see if they were also spatially poised to deliver signals to the wound bed. To identify LCs in skin tissue, I generated a powerful genetic mouse model,

LC-iGFP mice, in which treatment with a low dose of tamoxifen induced membrane-associated GFP expression in LCs. This model had two key advantages: it labeled LCs with high efficiency and specificity, and the labeling was temporally controlled. By administering tamoxifen prior to wounding the mice, I was able to label only mature, resident LCs present in the naive tissue and then track their localization during wound healing. With this experimental design, I am confident that the GFP+ cells in both the epidermal and the dermal regions of the wound were true LCs that were present in the skin prior to injury, and were not Langerin+ dDCs nor newly arriving monocyte-derived LCs (Merad et al., 2008).

Using this mouse model, we learned that LCs persist in the skin after injury and localize at the epidermal and dermal edges of wound beds. This differs from how LCs respond to other inflammatory insults, including UV radiation (Noonan *et al.,* 1984) and tape stripping injury (Holzmann et al., 2004), in which the majority of LCs emigrate from the skin to the skin-draining lymph nodes. In fact, my flow cytometry data from wild type mice showed that the relative number of LCs in the epidermis increased as wound healing progressed. This increase in LCs could be due to migration of resident LCs toward the wound edge, proliferation of local LCs, or the arrival of new LCs from circulating precursor cells (Merad et al., 2008). Future studies using LC-iGFP mice and EdU proliferation assays will be designed to determine the source of these new LCs.

Immunostaining of LC-iGFP wound bed cross-sections revealed that LCs localize near CD31+ endothelial cells at the dermal edges of wounds. We were excited to see LCs positioned so close to blood vessels, where they could

potentially provide growth signals to stimulate angiogenesis. Since blood vessels exist in a 3D, highly-branched network in the skin, I also performed whole mount immunofluorescence staining, tissue clearing, and confocal microscopy of LC-iGFP wounds to better understand where along the vessels LCs were localized. This imaging illustrated that LCs were congregated at the leading epithelial edges of skin wounds, and many LCs were in close proximity to blood vessel tips. Endothelial tip cells function as vascular stem cells, and direct vascular outgrowth into wounds by sensing chemotactic gradients of angiogenic factors, such as VEGF (Johnson and Wilgus, 2014). Thus, the nearness of LCs to EC tip cells positions them to supply critical growth signals that drive and direct revascularization into regenerating wounds.

Our discovery that LCs localize at the growing tips of blood vessels during wound healing draws a novel functional parallel between LCs and macrophages. Macrophages have been shown to home to EC tip cells to regulate different angiogenic functions, including promoting tip cell fusion in the developing mouse brain (Fantin et al., 2010) and stabilizing vessel sprouting during zebrafish wound healing (Gurevich et al., 2018). My confocal imaging revealed that LCs localize at blood vessel tips similarly to these angiogenesis-promoting macrophages. These findings add new, compelling evidence to the debate whether LCs are more similar to macrophages than DCs (Doebel et al., 2017).

Together, my microscopy and flow cytometry data illuminated that LCs surround and infiltrate healing wounds, and specifically position themselves near blood vessels. In future studies to further validate and characterize the spatial

relationship between LCs and EC tip cells, I would label tip cells with a fluorescent antibody that targets Endothelial cell-specific molecule 1 (ESM1) and then capture high magnification z-stack images of LCs and tip cells at the wound edges. This experiment would enable me to visualize LCs and tip cells in high resolution and distinguish if the cells are physically touching or simply exist in the immediate vicinity of one another. To observe LC migration to blood vessel tips, I would perform *in vital* imaging in healing mouse wounds. Using fluorescent reporter mice, in which LCs and blood vessels express distinct fluorescent labels, I would be fascinated to observe the process of LC migration to the wound edges. Additionally, it would be fruitful to see if LCs remain associated with blood vessels and contribute to blood vessel remodeling later in wound healing.

Langerhans cells play an important functional role in skin angiogenesis and repair.

Our data reveal the previously unappreciated function of LCs in promoting angiogenesis after skin wounding. To determine the importance of LCs for skin repair, I characterized many facets of tissue repair in *huLang*-DTA mice, in which LCs are specifically and constitutively depleted while other dDC populations are spared (Kaplan et al., 2005). Broadly, we observed that LCs are important for the recruitment of endothelial cells and fibroblasts, but not immune cells or keratinocytes, to wounds. We were surprised by these results, as we had hypothesized that LCs would primarily signal to the cells in their immediate environment (keratinocytes) and other immune cells. We did observe that the

relative abundance of T cells was modestly elevated in 3-day *huLang*-DTA+ wounds compared to littermate controls, but we do not think this difference is driving the other wound healing phenotypes because the absolute number of T cells per wound is not significantly different between conditions.

It is important to note that these data speak to cell recruitment, but not directly to cell activation or function. A compelling area of future research would be to more thoroughly characterize the functions of different skin cell types in *huLang*-DTA wounds vs. controls. Transcriptomic and secretomic assays could be used to fully describe how endothelial cells, fibroblasts, keratinocytes, macrophages, and other skin cell types behave differently in the absence of LC-derived signals. These analyses could potentially reveal, for example, that while similar numbers of immune cells are recruited to *huLang*-DTA+ and DTA- wounds, the cells are differentially activated and secrete different cytokine profiles. Supplementally, transcriptomic and epigenetic characterization (using RNA-seq and ATAC-seq, respectively) of naive skin could be performed to determine if LCs prime the skin to better respond to injury.

By applying our tissue clearing and confocal imaging techniques to *huLang*-DTA wounds, we were able to visualize the extent to which the vasculature of LC-null wounds was morphologically defective. Two striking differences between the LC-depleted and control wounds were in (I) vessel growth into the wound and (II) vessel remodeling at the wound edges. While the control wounds were densely populated with CD31+ blood vessels extending toward the wound center, the wounds from *huLang*-DTA+ mice had much sparser vascular coverage and fewer

vessel tips per mm around the leading vascular edge. The control wounds also exhibited clear signs of vessel remodeling, as evident by the joining of small wound-edge capillaries into larger vessels at the wound periphery. In contrast, *huLang*-DTA+ wounds contained primarily thin capillaries, with little to no evidence of these small vessels joining to form larger arteries. Together, these morphological defects illuminate that LC-deficient mice exhibit defective blood vessel growth and arteriogenesis during wound-induced angiogenesis.

The data from my EdU pulse-chase experiments provided further evidence that EC proliferation is abrogated during wound healing in *huLang*-DTA+ mice. I maximally labeled proliferating ECs by administering twice-daily injections of EdU during the height of EC proliferation (3 and 4 days post-injury), and observed significantly less EdU incorporation into ECs from *huLang*-DTA+ wounds compared to littermate controls. Interestingly, stunted proliferation was specific to ECs; fibroblasts and immune cells from *huLang*-DTA+ and DTA- mice incorporated EdU at similar rates. This, in combination with my LC-EC colocalization data, supports a potential cellular mechanism in which LCs deliver pro-angiogenic growth signals directly to endothelial tip cells to stimulate EC proliferation and vessel growth into wound beds.

To dig even deeper into the angiogenic phenotype in our *huLang*-DTA mice, I would design future experiments to further characterize the morphology of the vascular network. For example, I would measure blood vessel size, average vessel length, and vessel branching in different regions of the wound bed to capture quantitative differences in the vascular architecture. I would also stain

whole mount *huLang*-DTA wounds for markers that distinguish capillaries, arteries, veins, and lymphatic vessels to better understand the identities and maturation states of the CD31+ vessels in these wounds. Finally, I would repeat these assays in later timepoints after injury to elucidate if the skin possesses sufficient compensatory mechanisms to successfully re-cellularize, revascularize, and remodel new tissue in the absence of LCs.

Final Remarks

Altogether, this body of work elucidates a novel function of Langerhans cells as a critical component of the skin's complex and heterogeneous angiogenic niche. We have established that LCs play a critical role in the regeneration and organization of new blood vessels, as well as the repopulation of fibroblasts into skin wounds. By taking a systems-level approach to discovering angiogenic signals in the skin, we were able to shed light on the angiogenic potential of previously unappreciated cell types and signaling ligands. We hope that our work serves as a valuable resource for the discovery of new angiogenic regulators and therapeutic targets for the treatment of chronic, non-healing skin wounds.

Chapter 6: Materials and Methods

Animals

Wild-type C57BL6/J mice were purchased from Charles River. B6.FVB-Tg(CD207-Dta)312Dhka/J (*huLang*-DTA); Tg(CD207-cre/ERT2)1Dhka/J (huLang-CreER); and B6.129(Cg)-Gt(ROSA)26Sortm4(ACTB-tdTomato,-EGFP)Luo/J (mT/mG) mice were purchased from The Jackson Laboratories. Mice were maintained through routine breeding in an Association for Assessment and Accreditation of Laboratory Animal Care (AALAC)-accredited animal facility at Yale University. Animals were maintained on a standard chow diet ad libitum (Harlan Laboratories, 2018S) in 12-hour light/dark cycling. Two or three injured mice were housed per cage. All experimental procedures were approved and in accordance with the Yale University Institutional Animal Care and Use Committee.

Lineage tracing and EdU treatment

To label Langerhans cells, *huLangerin*-CreER; mT/mG mice received daily intraperitoneal (i.p.) injections of 50 µL of 30mg/mL tamoxifen (Sigma Aldrich) in sesame oil for 3 days.

For EdU experiments, 50mg/kg of EdU (Invitrogen) was injected intraperitoneally at indicated time points and detected per manufacturer protocols. Detection of EdU-incorporating cells was performed using Click-it EdU Imaging or Flow Cytometry Assay kits (Invitrogen).

Wound healing models

RNA sequencing data from Haensel et al. (2020) (GSE142471) utilized a 6-mm punch biopsy to induce wounding and analyzed the proliferative phase of wound repair at day 4. The RNA sequencing data from wounds purified for CD45+ cells (GSE166950) and all other skin wound analyses utilized a 4-mm punch biopsy model. The proliferative phase of wound repair begins at day 4 and day 3 for the 6-mm and 4-mm wound models, respectively.

For all histological and FACS data, 7-9-week-old mice were wounded during the telogen phase of hair cycling. Mice were anesthetized using isoflurane and wounds were created on shaved back skin using a 4mm biopsy punch (Accuderm). Animals were sacrificed at noted intervals after injury and wound beds were processed for subsequent analysis.

Immunofluorescence and imaging

Skin sections: Mouse skin and wound beds were embedded in O.C.T. and wound beds were sectioned through their entirety to identify the center. 14 μm cryosections were processed as previously described (Shook et al., 2016) and stained with antibodies listed in the Key Resources Table. Histological quantification for each wound bed was conducted on the three central-most sections and the averages from two wounds were averaged for each animal. Composite images were acquired using the tiles module on a Zeiss AxioImager M1 (Zeiss) equipped with an Orca camera (Hamamatsu). Tiled and stitched images of wound sections were collected using a 20X objective, controlled by Zen software (Carl Zeiss). The percentage of the wound bed covered by DAPI staining

(re-epithelialization), width of the wound bed, and ER-TR7 corrected total fluorescence were calculated from the 3 central most tissue sections using ImageJ software (National Institutes of Health, Bethesda, MD) as described previously (Schmidt and Horsley, 2013; Shook et al., 2018). Revascularization (CD31+) was calculated using Adobe Photoshop to measure the total pixels positive for antibody staining divided by the total number of pixels in wound beds. EdU labeling was performed using the Click-iT EdU™ Cell Proliferation Kit for Imaging per the manufacturer's instructions (Invitrogen).

Skin whole mount: Staining of whole mount adult mouse back skin was adapted from (Gur-Cohen et al., 2019). Briefly, mice were euthanized and their back skin was chemically depilated (Nair, 5 minutes) and then cleansed with 70% ethanol. A 6mm-diameter biopsy punch was used to excise nonwounded back skin or wounds (captures 4mm wound with a 1mm border of surrounding nonwounded skin). Tissue was placed dermis-down on Whatman paper and fixed in 4% formaldehyde in PBS for 1 hour at room temperature, followed by extensive washing with PBS. Tissue was permeabilized with 0.3% Triton X-100 in PBS (PBS-T) overnight at 4˚C, followed by incubation in blocking buffer (1% fish gelatin, 2.5% normal donkey serum, 2.5% normal goat serum, 1% BSA, 0.3% PBS-T) for 3-4 hours at room temperature. For immunolabeling, primary antibodies were incubated at room temperature overnight, followed by hourly washes with 0.3% PBS-T for 5 hours. Secondary antibodies conjugated to Alexa Fluor™ 488, RRX, or 647 (1:300, Invitrogen), were incubated at room temperature overnight, followed by hourly PBS-T washes for 5 hours, proceeded by tissue clearing.

Tissue clearing: Tissue clearing was adapted from Gur-Cohen *et al.* (2019) (Gur-Cohen *et al.*, 2019). Briefly, immunostained back skin tissues were dehydrated in increasing concentrations of ethanol (30%, 50%, and 70%, diluted in distilled water and adjusted to pH 9.0) for 45-60 minutes each at room temperature and with gentle agitation. Samples were then incubated in 2 rounds of 100% ethanol (no pH adjustment) for 60 minutes each, at room temperature with gentle agitation. Dehydrated samples were transferred into 500 µL ethyl cinnamate (Sigma) in polypropylene tubes for clearing overnight at room temperature. To acquire images, cleared skin was mounted dermis-down with ethyl cinnamate in a glass bottom microwell dish (35mm, MatTek) held in place with a coverslip (22 mm x 22 mm, Fisher Scientific).

Confocal microscopy: Confocal images were acquired using a Zeiss LSM 880 confocal microscope. The LSM 980 confocal microscope is equipped with Zeiss Axio Observer Z1 inverted microscope with 405, 458, 488, 514, 561, and 633 laser lines, and Zen software (Zeiss). Stacks of 4-13 µm steps were collected (step sized determined by setting pinhole opening to 1 Airy Unit) with a 10x or 20x objective. Imaging data stitching, processing, and rendering was performed in ZEN (ZEISS) and FIJI (NIH). FIJI software was used to generate maximum intensity projections and 3D renderings of z-stacks.

Flow cytometry and Cell Sorting

For all flow cytometry experiments, mouse back skin and wound beds were dissected and digested into a single cell suspension, resuspended in FACS

staining buffer (1% BSA in PBS with 2mM EDTA), and then filtered with a 70 mm and a 40 mm cell strainer prior to centrifugation. Cell suspensions were stained with antibodies purchased from eBioscience, Biolegend, and BD Bioscience in the Key Resources Table for 20-30 minutes on ice, washed, and then analyzed on the flow cytometer. Flow cytometry analysis was performed using FlowJo Software (FlowJo).

Immunophenotyping analysis: For the quantification of myeloid cells and T cells, skin tissue was digested using Liberase TM (Roche). To exclude dead cells, Sytox Orange or Sytox Blue (Invitrogen, 1:1000) was added immediately before analysis. Flow cytometry was performed on a FACS Aria III with FACS DiVA software (BD Biosciences).

Dermal analysis: For the analysis of dermal cell types (endothelial cells and fibroblasts), skin tissue was digested using Collagenase 1 (Worthington). Analysis of proliferation using EdU incorporation was performed using the Click-iT^{TM} EdU Flow Cytometry Assay Kit per the manufacturer's instructions (Invitrogen). Flow cytometry was performed on a BD FACS LSR Fortessa X20 with FACS DiVA software (BD Biosciences).

Epidermal cell analysis: For the analysis of LCs in epidermal tissue, we adapted the protocol from (Soteriou et al., 2016). In short, naive skin or wound beds were dissected and the underlying facia and adipose tissue were scraped off. Skin pieces were floated dermis-down on 0.25% Trypsin-EDTA (Gibco) at 37˚C for 30-60 minutes, and then epidermal cells were gently scraped in the direction of hair growth into the solution. Cells were then washed, pelleted, and stained as

described. To exclude dead cells, Sytox Orange or Sytox Blue (Invitrogen, 1:1000) was added immediately before analysis. Flow cytometry was performed on a FACS Aria III with FACS DiVA software (BD Biosciences).

Single-cell RNA-sequencing data analysis

Data for GSE166950: Unwounded skin or wound beds with 0.25 mm perimeter of adjacent nonwounded skin were excised and digested in Liberase TL (Sigma) at 37℃ for 2.5 hours. After placing samples on ice and adding EDTA and FBS, digested tissues were mechanically disrupted by syringe plunger and then filtered through a 70-micron filter to exclude tissue debris and obtain a single cell suspension for downstream analyses.

Single cell suspensions were stained with anti-CD16/32 before staining with surface fluorescent conjugated antibodies and/or oligo-tagged antibodies at predetermined concentrations in a 100 µL staining buffer (PBS containing 5% FBS and 1% HEPES) per 10^7 cells. Stained cells were re-suspended in 4',6-diamidino-2-phenylindole (DAPI) in FACS buffer (Sigma-Aldrich) prior to analysis. Data were acquired on LSRII Analyzers (BD Biosciences) and then analyzed with FlowJo program. Fluorescence-activated cell sorting (FACS) was conducted using Aria Cell Sorters (BD Biosciences).

FACS purified live CD45.2$^+$ CD90.2$^+$ TCR Vγ3 $^-$ cells from unwounded skin, 3 and 5 days post wounding were prelabeled with surface epitope marking oligo-tagged antibodies and sample specific oligo-tagged Totalseq-A antibodies (Biolegend, see table 1). Hashed samples were pooled at Ctrl,1: D3,1.5, D5:1 ratio

prior to library preparation (Chromium Single Cell 3′ Library, 10x Genomics) and sequenced on an Illumina HiSeq 4000 as 150 bp paired-end reads. Sequencing results were demultiplexed and converted to FASTQ format using Illumina bcl2fastq software. The Cell Ranger Single-Cell Software Suite (https://support.10xgenomics.com/single-cell-gene-expression/software/pipelines/latest/what-is-cell-ranger) was used to perform sample demultiplexing, barcode processing, and single-cell 3' gene counting. The cDNA insert was aligned to the mm10/GRCm38 reference genome. Only confidently mapped, non-PCR duplicates with valid barcodes and UMIs were used to generate the gene-barcode matrix. Cell Ranger output was further analyzed in R using the Seurat package (Butler et al., 2018). Surface epitope oligo sequences were merged with cell transcriptome data by matching the cell barcode IDs.

Further analysis including quality filtering, the identification of highly variable genes, dimensionality reduction, standard unsupervised clustering algorithms, and the discovery of differentially expressed genes was performed using the Seurat R package. Samples were demultiplexed to filter out multiplets (cells mapping to multiple hashtags) and negative cells (cells missing hashtags) with a positive quantile threshold of 0.99 between samples. Individual samples were further processed to remove cells with > 20% mitochondrial gene expression. To exclude low quality cells and remaining multiplets or cells that were extreme outliers, we calculated the distribution of total genes/ cells. Following that, we applied control parameters to filter cells with fewer than 200 detected genes and more than 3800 detected genes. After removing unwanted cells from the dataset, we normalized

the data by the total expression, multiplied by a scale factor of 10,000, and log-transformed the result.

The downstream analysis was performed in R programming environment and primarily using the Seurat package (Hao et al., 2021).The hashtag data was first demultiplexed using Seurat demultiplexing where the HTO data was normalized using centered log ratio transformation (CLR) followed by HTODemux function with positive quantile set to (0.99). The HTO demultiplexed data was further subset to only include the singlets. The RNA data was further filtered using standard QC steps where cells with number of genes less than 200 and greater 4500 were filtered out to remove any low-quality cells and any remaining doublets. Cells with overall mitochondrial gene expression greater 20% were also filtered to remove cells with poor survival rate.

Followed by quality control filtering, we performed standard data processing on RNA seq assay including normalization, scaling and PCA. First clustering results were generated using the first 7 dimensions and resolution set to 0.3 for the FindClusters function. UMAP plot (Fig. 2A) was generated using these results and the resulting 12 clusters were annotated using marker genes identified after using FindAllMarkers function and using predefined marker genes for each cell type (Fig. 2A, Fig. S2C). Feature expression plots were also generated for genes of interest using FeaturePlot function (Fig. 2B, Fig. S2C-D).

Data analysis of GSE142471: Data from Haensel et al. (2020) was first preprocessed to remove low quality cells using Seurat tools adapted for Python (Scanpy)(Wolf et al., 2018), and then log-normalized to convert mRNA counts to

gene expression. Dimensionality reduction and visualization were accomplished using the Scanpy implementation of Uniform Manifold Approximation and Projection (UMAP)(Wolf *et al.*, 2018)). To label the data by broad cell type, we adapted the annotation pipeline from (Kumar et al., 2018) to use a simple feedforward neural network (NN). The NN was built with the TensorFlow module in Python (https://www.tensorflow.org/). Differentially expressed genes (DEGs) across wounding conditions were identified using the diffxpy package ($log_2FC > 1$ and adjusted p-value < 0.05). Enrichment analysis on the top DEGs was performed using the Generally Applicable Gene-set Enrichment (GAGE) package in R (Luo et al., 2009). Gene Ontology (GO) biological processes and the Kyoto Encyclopedia of Genes and Genomes (KEGG) were used as reference databases.

To characterize potential signaling to endothelial cells (ECs) from scRNA-seq, we took advantage of the NicheNet algorithm, which makes inferences about ligand binding from patterns in expression of target genes in receiving cells (Browaeys et al., 2020). Target genes in the EC population were identified as genes significantly upregulated after wounding ($log_2FC > 0.25$ and adjusted p-value < 0.05). NicheNet is available as an open-source software package in R.

For single-cell measurements, statistics were generally performed using two-sided Wilcoxon rank-sum tests and the Benjamini-Hochberg method of correction for pairwise multiple comparisons, or as specified in the figure legends. Values were considered significant at $P < 0.05$. Analyses were performed using custom Python and R scripts.

Table 2: Key Resource Table

REAGENT or RESOURCE	SOURCE	IDENTIFIER
Antibodies		
APC/eFluor 780 anti-mouse CD45 rat monoclonal	eBioscience	Cat# 47-0451-82; RRID: AB_1548781 (Clone 30-F11)
Alexa Fluor 700 anti-mouse CD11b rat monoclonal	eBioscience	Cat# 56-0112-82; RRID: AB_657585 (Clone M1/70)
eFluor 450 anti-mouse F4/80 rat monoclonal	eBioscience	Cat# 48-4801-82; RRID: AB_1548747 (Clone BM8)
PE/Cy7 anti-mouse Ly6G rat monoclonal (clone 1A8)	Biolegend	Cat# 127618; RRID: AB_1877261
APC anti-mouse Ly6C rat monoclonal (clone HK1.4)	eBioscience	Cat# 17-5932; RRID: AB_1724155
Alexa Fluor 488 anti-mouse CD206 rat monoclonal	Biolegend	Cat# 141710; RRID: AB_10900445 (clone C068C2)
PE anti-mouse MHCII rat monoclonal	eBioscience	Cat# 12-5321-82; AB_465928 (clone M5/114.15.2)
APC anti-mouse EpCam rat monoclonal (clone G8.8)	BD Biosciences	Cat# 563478; RRID: AB_2738234
PerCp/Cy5.5 anti-mouse CD64 rat monoclonal	Biolegend	Cat# 139308; RRID: AB_2561963 (clone X54-5/7.1)
FITC anti-mouse CD3e Armenian hamster	eBioscience	Cat# 11-0031-82; RRID: AB_464882 monoclonal (clone 145-2C11)
PerCp anti-mouse CD4 rat monoclonal (clone GK1.5)	Biolegend	Cat# 100434; RRID: AB_893324
APC anti-mouse CD8a rat monoclonal (clone 53-6.7)	eBioscience	Cat# 17-0081-83; RRID: AB_469336
PE anti-mouse gd-TCR Armenian hamster	BD Biosciences	Cat# 553178; RRID: AB_394689 monoclonal (clone GL3)

Alexa Fluor 700 anti-mouse CD29 Armenian hamster	Biolegend	Cat# 102218; RRID: AB_493711 monoclonal (clone HMbeta1-1)
Brilliant Violet 421 anti-mouse CD34 rat monoclonal	Biolegend	Cat# 119321; RRID: AB_10900980 (clone MEC14.7)
APC-Fire750 anti-mouse CD31 rat monoclonal (390)	Biolegend	Cat# 102434; RRID: AB_2629683
Anti-CD31 (PECAM-1) Armenian hamster monoclonal	Millipore	Cat# MAB1398Z, RRID:AB_94207 (clone 2H8)
Rat Anti-Mouse CD31, Clone MEC 13.3 (RUO)	BD Biosciences	Cat# 550274, RRID: AB_393571
Anti-ER-TR7 rat monoclonal	Abcam	Cat# ab51824; RRID: AB_881651
Anti-GFP chicken polyclonal	Abcam	Cat# ab13970; RRID: AB_300798
Anti-mouse/human CD207 (Langerin) Antibody	BioLegend	Cat# 144202; AB_2562088
Chemicals, Peptides, and Recombinant Proteins		
Tamoxifen	Sigma	T5648
EdU (5-ethynyl-2'-deoxyuridine)	Invitrogen	E10187
Sytox Orange	Invitrogen	S34861
Sytox Blue	Invitrogen	S34857
Collagenase 1	Worthington	LS004196
Liberase TM	Roche	5401127001
Liberase TL	Roche	5401020001
Ethyl cinnamate	Sigma-Aldrich	112372
Critical Commercial Assays		

Click-iT EdU Alexa Fluor 647 Flow Cytometry Assay Kit	Invitrogen	C10419
Click-iT EdU Alexa Fluor 647 Imaging Kit	Invitrogen	C10340
Experimental Models: Organisms/Strains		
Mouse: C57BL/6	Charles River	027
Mouse: B6.FVB-Tg(CD207-Dta)312Dhka/J	The Jackson Laboratory	017949
Mouse: Tg(CD207-cre/ERT2)1Dhka/J	The Jackson Laboratory	028287
Mouse: B6.129(Cg)-Gt(ROSA)26Sortm4(ACTB-tdTomato,-EGFP)Luo/J	The Jackson Laboratory	007676
Software and Algorithms		
Fiji (ImageJ)	NIH	https://fiji.sc
Adobe Photoshop	Adobe	https://www.adobe.com/products/photoshop.html
FlowJo	FlowJo, LLC	https://www.flowjo.com
GraphPad Prism	GraphPad Software, Inc	https://www.graphpad.com
Scanpy	Python	https://github.com/theislab/scanpy
Tensorflow	Python	https://www.tensorflow.org
NicheNet	R	https://github.com/saeyslab/nichenetr
Circlize (for chord diagram visualization)	R	https://github.com/jokergoo/circlize
Seurat 3.0	Stuart et al., 2019	https://satijalab.org/seurat/

References

Adams, R.H., and Alitalo, K. (2007). Molecular regulation of angiogenesis and lymphangiogenesis. Nat Rev Mol Cell Biol *8*, 464-478. 10.1038/nrm2183.

Alcolea MP, Jones PH. Lineage analysis of epidermal stem cells. Cold Spring Harb Perspect Med. 2014;4(1):a015206. Published 2014 Jan 1. doi:10.1101/cshperspect.a015206

Arwert EN, Hoste E, Watt FM. Epithelial stem cells, wound healing and cancer. Nat Rev Cancer. 2012;12(3):170-180. Published 2012 Feb 24. doi:10.1038/nrc3217

Barrientos S, Stojadinovic O, Golinko MS, Brem H, Tomic-Canic M. Growth factors and cytokines in wound healing. Wound Repair Regen. 2008;16(5):585-601. doi:10.1111/j.1524-475X.2008.00410.x

Bikle DD. Vitamin D metabolism and function in the skin. *Mol Cell Endocrinol.* 2011;347(1-2):80-89. doi:10.1016/j.mce.2011.05.017

Bobr, A., Igyarto, B.Z., Haley, K.M., Li, M.O., Flavell, R.A., and Kaplan, D.H. (2012). Autocrine/paracrine TGF-β1 inhibits Langerhans cell migration. Proc Natl Acad Sci U S A 109, 10492-10497. 10.1073/pnas.1119178109.

Bobr A, Olvera-Gomez I, Igyarto BZ, Haley KM, Hogquist KA, Kaplan DH. Acute ablation of Langerhans cells enhances skin immune responses. J Immunol. 2010;185(8):4724-4728. doi:10.4049/jimmunol.1001802

Bocheva G, Slominski RM, Janjetovic Z, et al. Protective Role of Melatonin and Its Metabolites in Skin Aging. *Int J Mol Sci.* 2022;23(3):1238. Published 2022 Jan 22. doi:10.3390/ijms23031238

Bosisio, D., Ronca, R., Salvi, V., Presta, M., and Sozzani, S. (2018). Dendritic cells in inflammatory angiogenesis and lymphangiogenesis. Curr Opin Immunol 53, 180-186. 10.1016/j.coi.2018.05.011.

Bosurgi L, Cao YG, Cabeza-Cabrerizo M, et al. Macrophage function in tissue repair and remodeling requires IL-4 or IL-13 with apoptotic cells. Science. 2017;356(6342):1072-1076. doi:10.1126/science.aai8132

Browaeys, R., Saelens, W., and Saeys, Y. (2020). NicheNet: modeling intercellular communication by linking ligands to target genes. Nat Methods 17, 159-162. 10.1038/s41592-019-0667-5.

Bursch LS, Wang L, Igyarto B, et al. Identification of a novel population of Langerin+ dendritic cells. J Exp Med. 2007;204(13):3147-3156. doi:10.1084/jem.20071966

Butler, A., Hoffman, P., Smibert, P., Papalexi, E., and Satija, R. (2018). Integrating single-cell transcriptomic data across different conditions, technologies, and species. Nat Biotechnol 36, 411-420. 10.1038/nbt.4096.

Bynoe MS, Evans JT, Viret C, Janeway CA Jr. Epicutaneous immunization with autoantigenic peptides induces T suppressor cells that prevent experimental allergic encephalomyelitis. Immunity. 2003;19(3):317-328. doi:10.1016/s1074-7613(03)00239-5

Carmeliet P, Jain RK. Molecular mechanisms and clinical applications of angiogenesis. Nature. 2011;473(7347):298-307. doi:10.1038/nature10144

Charkoudian N. Skin blood flow in adult human thermoregulation: how it works, when it does not, and why. *Mayo Clin Proc.* 2003;78(5):603-612. doi:10.4065/78.5.603

Clausen BE, Kel JM. Langerhans cells: critical regulators of skin immunity?. Immunol Cell Biol. 2010;88(4):351-360. doi:10.1038/icb.2010.40

Curiel, T.J., Cheng, P., Mottram, P., Alvarez, X., Moons, L., Evdemon-Hogan, M., Wei, S., Zou, L., Kryczek, I., Hoyle, G., et al. (2004). Dendritic cell subsets differentially regulate angiogenesis in human ovarian cancer. Cancer Res 64, 5535-5538. 10.1158/0008-5472.CAN-04-1272.

Dąbrowska AK, Spano F, Derler S, Adlhart C, Spencer ND, Rossi RM. The relationship between skin function, barrier properties, and body-dependent factors. *Skin Res Technol.* 2018;24(2):165-174. doi:10.1111/srt.12424

DeLisser, H.M., Christofidou-Solomidou, M., Strieter, R.M., Burdick, M.D., Robinson, C.S., Wexler, R.S., Kerr, J.S., Garlanda, C., Merwin, J.R., Madri, J.A., and Albelda, S.M. (1997). Involvement of endothelial PECAM-1/CD31 in angiogenesis. Am J Pathol 151, 671-677.

Doebel T, Voisin B, Nagao K. Langerhans Cells - The Macrophage in Dendritic Cell Clothing. Trends Immunol. 2017;38(11):817-828. doi:10.1016/j.it.2017.06.008

Eming, S.A., Brachvogel, B., Odorisio, T., and Koch, M. (2007). Regulation of angiogenesis: wound healing as a model. Prog Histochem Cytochem 42, 115-170. 10.1016/j.proghi.2007.06.001.

Eming SA, Krieg T, Davidson JM. Inflammation in wound repair: molecular and cellular mechanisms. J Invest Dermatol. 2007;127(3):514-525. doi:10.1038/sj.jid.5700701

Eming SA, Martin P, Tomic-Canic M. Wound repair and regeneration: mechanisms, signaling, and translation. Sci Transl Med. 2014;6(265):265sr6. doi:10.1126/scitranslmed.3009337

Falanga, V. (2005). Wound healing and its impairment in the diabetic foot. Lancet 366, 1736-1743. 10.1016/S0140-6736(05)67700-8.

Fan, Y., Arif, A., Gong, Y., Jia, J., Eswarappa, S.M., Willard, B., Horowitz, A., Graham, L.M., Penn, M.S., and Fox, P.L. (2012). Stimulus-dependent phosphorylation of profilin-1 in angiogenesis. Nat Cell Biol 14, 1046-1056. 10.1038/ncb2580.

Fantin A, Vieira JM, Gestri G, et al. Tissue macrophages act as cellular chaperones for vascular anastomosis downstream of VEGF-mediated endothelial tip cell induction. Blood. 2010;116(5):829-840. doi:10.1182/blood-2009-12-257832

Festa E, Fretz J, Berry R, et al. Adipocyte lineage cells contribute to the skin stem cell niche to drive hair cycling. Cell. 2011;146(5):761-771. doi:10.1016/j.cell.2011.07.019

Flacher V, Bouschbacher M, Verronèse E, et al. Human Langerhans cells express a specific TLR profile and differentially respond to viruses and Gram-positive bacteria. J Immunol. 2006;177(11):7959-7967. doi:10.4049/jimmunol.177.11.7959

Figdor CG, van Kooyk Y, Adema GJ. C-type lectin receptors on dendritic cells and Langerhans cells. Nat Rev Immunol. 2002;2(2):77-84. doi:10.1038/nri723

Giacca M, Zacchigna S. VEGF gene therapy: therapeutic angiogenesis in the clinic and beyond. Gene Ther. 2012;19(6):622-629. doi:10.1038/gt.2012.17

Gomez de Agüero M, Vocanson M, Hacini-Rachinel F, et al. Langerhans cells protect from allergic contact dermatitis in mice by tolerizing CD8(+) T cells and activating Foxp3(+) regulatory T cells. J Clin Invest. 2012;122(5):1700-1711. doi:10.1172/JCI59725

Gonzalez AC, Costa TF, Andrade ZA, Medrado AR. Wound healing - A literature review. An Bras Dermatol. 2016;91(5):614-620. doi:10.1590/abd1806-4841.20164741

Gur-Cohen, S., Yang, H., Baksh, S.C., Miao, Y., Levorse, J., Kataru, R.P., Liu, X., de la Cruz-Racelis, J., Mehrara, B.J., and Fuchs, E. (2019). Stem cell–driven lymphatic remodeling coordinates tissue regeneration. Science 366, 1218-1225. 10.1126/science.aay4509.

Gurevich DB, Severn CE, Twomey C, et al. Live imaging of wound angiogenesis reveals macrophage orchestrated vessel sprouting and regression. EMBO J. 2018;37(13):e97786. doi:10.15252/embj.201797786

Haensel, D., Jin, S., Sun, P., Cinco, R., Dragan, M., Nguyen, Q., Cang, Z., Gong, Y., Vu, R., MacLean, A.L., et al. (2020). Defining Epidermal Basal Cell States during Skin Homeostasis and Wound Healing Using Single-Cell Transcriptomics. Cell Rep 30, 3932-3947.e3936. 10.1016/j.celrep.2020.02.091.

Hamik, A., Wang, B., and Jain, M.K. (2006). Transcriptional regulators of angiogenesis. Arterioscler Thromb Vasc Biol 26, 1936-1947. 10.1161/01.ATV.0000232542.42968.e3.

Hao, Y., Hao, S., Andersen-Nissen, E., Mauck, W.M., Zheng, S., Butler, A., Lee, M.J., Wilk, A.J., Darby, C., Zager, M., et al. (2021). Integrated analysis of multimodal single-cell data. Cell 184, 3573-3587.e3529. 10.1016/j.cell.2021.04.048.

Herbert, S.P., and Stainier, D.Y. (2011). Molecular control of endothelial cell behaviour during blood vessel morphogenesis. Nat Rev Mol Cell Biol 12, 551-564. 10.1038/nrm3176.

Holzmann S, Tripp CH, Schmuth M, et al. A model system using tape stripping for characterization of Langerhans cell-precursors in vivo. J Invest Dermatol. 2004;122(5):1165-1174. doi:10.1111/j.0022-202X.2004.22520.x

Igyártó BZ, Haley K, Ortner D, et al. Skin-resident murine dendritic cell subsets promote distinct and opposing antigen-specific T helper cell responses. Immunity. 2011;35(2):260-272. doi:10.1016/j.immuni.2011.06.005

Igyarto, B.Z., and Kaplan, D.H. (2010). The evolving function of Langerhans cells in adaptive skin immunity. Immunol Cell Biol 88, 361-365. 10.1038/icb.2010.24.

Johnson KE, Wilgus TA. Vascular Endothelial Growth Factor and Angiogenesis in the Regulation of Cutaneous Wound Repair. Adv Wound Care (New Rochelle). 2014;3(10):647-661. doi:10.1089/wound.2013.0517

Kalucka, J., de Rooij, L.P.M.H., Goveia, J., Rohlenova, K., Dumas, S.J., Meta, E., Conchinha, N.V., Taverna, F., Teuwen, L.A., Veys, K., et al. (2020). Single-Cell Transcriptome Atlas of Murine Endothelial Cells. Cell 180, 764-779.e720. 10.1016/j.cell.2020.01.015.

Kaplan DH, Jenison MC, Saeland S, Shlomchik WD, Shlomchik MJ. Epidermal langerhans cell-deficient mice develop enhanced contact hypersensitivity. Immunity. 2005;23(6):611-620. doi:10.1016/j.immuni.2005.10.008

Kessler-Becker D, Krieg T, Eckes B. Expression of pro-inflammatory markers by human dermal fibroblasts in a three-dimensional culture model is mediated by an autocrine interleukin-1 loop. Biochem J. 2004;379(Pt 2):351-358. doi:10.1042/BJ20031371

Kobayashi T, Naik S, Nagao K. Choreographing Immunity in the Skin Epithelial Barrier. *Immunity*. 2019;50(3):552-565. doi:10.1016/j.immuni.2019.02.023

Kobayashi T, Voisin B, Kim DY, et al. Homeostatic Control of Sebaceous Glands by Innate Lymphoid Cells Regulates Commensal Bacteria Equilibrium. *Cell*. 2019;176(5):982-997.e16. doi:10.1016/j.cell.2018.12.031

Koh, T.J., Novak, M.L., and Mirza, R.E. (2013). Assessing macrophage phenotype during tissue repair. Methods Mol Biol 1037, 507-518. 10.1007/978-1-62703-505-7_30.

Kretzschmar K, Watt FM. Markers of epidermal stem cell subpopulations in adult mammalian skin. *Cold Spring Harb Perspect Med*. 2014;4(10):a013631. Published 2014 Jul 3. doi:10.1101/cshperspect.a013631

Krzyszczyk P, Schloss R, Palmer A, Berthiaume F. The Role of Macrophages in Acute and Chronic Wound Healing and Interventions to Promote Pro-wound Healing Phenotypes. Front Physiol. 2018;9:419. Published 2018 May 1. doi:10.3389/fphys.2018.00419

Kumar, M.P., Du, J., Lagoudas, G., Jiao, Y., Sawyer, A., Drummond, D.C., Lauffenburger, D.A., and Raue, A. (2018). Analysis of Single-Cell RNA-Seq Identifies Cell-Cell Communication Associated with Tumor Characteristics. Cell Rep 25, 1458-1468.e1454. 10.1016/j.celrep.2018.10.047.

Landén NX, Li D, Ståhle M. Transition from inflammation to proliferation: a critical step during wound healing. Cell Mol Life Sci. 2016;73(20):3861-3885. doi:10.1007/s00018-016-2268-0

Lau K, Paus R, Tiede S, Day P, Bayat A. Exploring the role of stem cells in cutaneous wound healing. Exp Dermatol. 2009;18(11):921-933. doi:10.1111/j.1600-0625.2009.00942.x

Lumpkin EA, Caterina MJ. Mechanisms of sensory transduction in the skin. *Nature*. 2007;445(7130):858-865. doi:10.1038/nature05662

Luo, W., Friedman, M.S., Shedden, K., Hankenson, K.D., and Woolf, P.J. (2009). GAGE: generally applicable gene set enrichment for pathway analysis. BMC Bioinformatics 10, 161. 10.1186/1471-2105-10-161.

Ma Y, Yabluchanskiy A, Iyer RP, et al. Temporal neutrophil polarization following myocardial infarction. Cardiovasc Res. 2016;110(1):51-61. doi:10.1093/cvr/cvw024

Macleod AS, Havran WL. Functions of skin-resident γδ T cells. *Cell Mol Life Sci.* 2011;68(14):2399-2408. doi:10.1007/s00018-011-0702-x

Mansfield K, Naik S. Unraveling Immune-Epithelial Interactions in Skin Homeostasis and Injury. *Yale J Biol Med*. 2020;93(1):133-143. Published 2020 Mar 27.

Martin P, Gurevich DB. Macrophage regulation of angiogenesis in health and disease. Semin Cell Dev Biol. 2021;119:101-110. doi:10.1016/j.semcdb.2021.06.010

Merad M, Ginhoux F, Collin M. Origin, homeostasis and function of Langerhans cells and other langerin-expressing dendritic cells. Nat Rev Immunol. 2008;8(12):935-947. doi:10.1038/nri2455

Mueller SN, Mackay LK. Tissue-resident memory T cells: local specialists in immune defense. *Nat Rev Immunol*. 2016;16(2):79-89. doi:10.1038/nri.2015.3

Muzumdar, M.D., Tasic, B., Miyamichi, K., Li, L., and Luo, L. (2007). A global double-fluorescent Cre reporter mouse. Genesis 45, 593-605. 10.1002/dvg.20335.

Nagao K, Ginhoux F, Leitner WW, et al. Murine epidermal Langerhans cells and langerin-expressing dermal dendritic cells are unrelated and exhibit distinct functions. Proc Natl Acad Sci U S A. 2009;106(9):3312-3317. doi:10.1073/pnas.0807126106

Natsuga K. Epidermal barriers. *Cold Spring Harb Perspect Med.* 2014;4(4):a018218. Published 2014 Apr 1. doi:10.1101/cshperspect.a018218

Newman, P.J., Berndt, M.C., Gorski, J., White, G.C., Lyman, S., Paddock, C., and Muller, W.A. (1990). PECAM-1 (CD31) cloning and relation to adhesion molecules of the immunoglobulin gene superfamily. Science 247, 1219-1222. 10.1126/science.1690453.

Nguyen AV, Soulika AM. The Dynamics of the Skin's Immune System. *Int J Mol Sci.* 2019;20(8):1811. Published 2019 Apr 12. doi:10.3390/ijms20081811

Noonan FP, Bucana C, Sauder DN, De Fabo EC. Mechanism of systemic immune suppression by UV irradiation in vivo. II. The UV effects on number and morphology of epidermal Langerhans cells and the UV-induced suppression of contact hypersensitivity have different wavelength dependencies. J Immunol. 1984;132(5):2408-2416.

Owens DM, Lumpkin EA. Diversification and specialization of touch receptors in skin. *Cold Spring Harb Perspect Med*. 2014;4(6):a013656. Published 2014 Jun 2. doi:10.1101/cshperspect.a013656

Pasparakis M, Haase I, Nestle FO. Mechanisms regulating skin immunity and inflammation. Nat Rev Immunol. 2014;14(5):289-301. doi:10.1038/nri3646

Phillipson M, Kubes P. The Healing Power of Neutrophils. Trends Immunol. 2019;40(7):635-647. doi:10.1016/j.it.2019.05.001

Plikus MV, Chuong CM. Macroenvironmental regulation of hair cycling and collective regenerative behavior. Cold Spring Harb Perspect Med.

2014;4(1):a015198. Published 2014 Jan 1. doi:10.1101/cshperspect.a015198

Potente M, Gerhardt H, Carmeliet P. Basic and therapeutic aspects of angiogenesis. Cell. 2011;146(6):873-887. doi:10.1016/j.cell.2011.08.039

Proksch E, Brandner JM, Jensen JM. The skin: an indispensable barrier. *Exp Dermatol.* 2008;17(12):1063-1072. doi:10.1111/j.1600-0625.2008.00786.x

Rahmani W, Sinha S, Biernaskie J. Immune modulation of hair follicle regeneration. NPJ Regen Med. 2020;5:9. Published 2020 May 11. doi:10.1038/s41536-020-0095-2

Rajesh A, Wise L, Hibma M. The role of Langerhans cells in pathologies of the skin. Immunol Cell Biol. 2019;97(8):700-713. doi:10.1111/imcb.12253

Rajesh A, Stuart G, Real N, et al. Depletion of langerin+ cells enhances cutaneous wound healing. Immunology. 2020;160(4):366-381. doi:10.1111/imm.13202

Rivera-Gonzalez G, Shook B, Horsley V. Adipocytes in skin health and disease. Cold Spring Harb Perspect Med. 2014;4(3):a015271. Published 2014 Mar 1. doi:10.1101/cshperspect.a015271

Romano E, Cotari JW, Barreira da Silva R, et al. Human Langerhans cells use an IL-15R-α/IL-15/pSTAT5-dependent mechanism to break T-cell tolerance against the self-differentiation tumor antigen WT1. Blood. 2012;119(22):5182-5190. doi:10.1182/blood-2011-09-382200

Roosterman D, Goerge T, Schneider SW, Bunnett NW, Steinhoff M. Neuronal control of skin function: the skin as a neuroimmunoendocrine organ. *Physiol Rev.* 2006;86(4):1309-1379. doi:10.1152/physrev.00026.2005

Rossiter H, Barresi C, Pammer J, et al. Loss of vascular endothelial growth factor a activity in murine epidermal keratinocytes delays wound healing and inhibits tumor formation. Cancer Res. 2004;64(10):3508-3516. doi:10.1158/0008-5472.CAN-03-2581

Schmidt, B.A., and Horsley, V. (2013). Intradermal adipocytes mediate fibroblast recruitment during skin wound healing. Development 140, 1517-1527. 10.1242/dev.087593.

Seré K, Baek JH, Ober-Blöbaum J, et al. Two distinct types of Langerhans cells populate the skin during steady state and inflammation. Immunity. 2012;37(5):905-916. doi:10.1016/j.immuni.2012.07.019

Sharma A, Saito Y, Hung SI, Naisbitt D, Uetrecht J, Bussiere J. The skin as a metabolic and immune-competent organ: Implications for drug-induced skin rash. *J Immunotoxicol*. 2019;16(1):1-12. doi:10.1080/1547691X.2018.1514444

Sheng, J., Chen, Q., Wu, X., Dong, Y.W., Mayer, J., Zhang, J., Wang, L., Bai, X., Liang, T., Sung, Y.H., et al. (2021). Fate mapping analysis reveals a novel murine dermal migratory Langerhans-like cell population. Elife 10. 10.7554/eLife.65412.

Shibuya M. Vascular Endothelial Growth Factor (VEGF) and Its Receptor (VEGFR) Signaling in Angiogenesis: A Crucial Target for Anti- and Pro-Angiogenic

Therapies. Genes Cancer. 2011;2(12):1097-1105. doi:10.1177/1947601911423031

Shook, B., Xiao, E., Kumamoto, Y., Iwasaki, A., and Horsley, V. (2016). CD301b+ Macrophages Are Essential for Effective Skin Wound Healing. J Invest Dermatol 136, 1885-1891. 10.1016/j.jid.2016.05.107.

Shook, B.A., Wasko, R.R., Rivera-Gonzalez, G.C., Salazar-Gatzimas, E., López-Giráldez, F., Dash, B.C., Muñoz-Rojas, A.R., Aultman, K.D., Zwick, R.K., Lei, V., et al. (2018). Myofibroblast proliferation and heterogeneity are supported by macrophages during skin repair. Science 362. 10.1126/science.aar2971.

Soteriou, D., Kostic, L., Sedov, E., Yosefzon, Y., Steller, H., and Fuchs, Y. (2016). Isolating Hair Follicle Stem Cells and Epidermal Keratinocytes from Dorsal Mouse Skin. J Vis Exp. 10.3791/53931.

Stockmann, C., Kirmse, S., Helfrich, I., Weidemann, A., Takeda, N., Doedens, A., and Johnson, R.S. (2011). A wound size-dependent effect of myeloid cell-derived vascular endothelial growth factor on wound healing. J Invest Dermatol 131, 797-801. 10.1038/jid.2010.345.

Stojadinovic O, Yin N, Lehmann J, Pastar I, Kirsner RS, Tomic-Canic M. Increased number of Langerhans cells in the epidermis of diabetic foot ulcers correlates with healing outcome. Immunol Res. 2013;57(1-3):222-228. doi:10.1007/s12026-013-8474-z

Stunova A, Vistejnova L. Dermal fibroblasts-A heterogeneous population with regulatory function in wound healing. Cytokine Growth Factor Rev. 2018;39:137-150. doi:10.1016/j.cytogfr.2018.01.003

Stutte, S., Jux, B., Esser, C., and Förster, I. (2008). CD24a expression levels discriminate Langerhans cells from dermal dendritic cells in murine skin and lymph nodes. J Invest Dermatol 128, 1470-1475. 10.1038/sj.jid.5701228.

Sun, Y., Lin, Z., Liu, C.H., Gong, Y., Liegl, R., Fredrick, T.W., Meng, S.S., Burnim, S.B., Wang, Z., Akula, J.D., et al. (2017). Inflammatory signals from photoreceptor modulate pathological retinal angiogenesis via c-Fos. J Exp Med 214, 1753-1767. 10.1084/jem.20161645.

Sunuwar, L., Asraf, H., Donowitz, M., Sekler, I., and Hershfinkel, M. (2017). The Zn. Biochim Biophys Acta Mol Basis Dis 1863, 947-960. 10.1016/j.bbadis.2017.01.009.

Ucuzian AA, Gassman AA, East AT, Greisler HP. Molecular mediators of angiogenesis. J Burn Care Res. 2010;31(1):158-175. doi:10.1097/BCR.0b013e3181c7ed82

Varricchi G, Granata F, Loffredo S, Genovese A, Marone G. Angiogenesis and lymphangiogenesis in inflammatory skin disorders. J Am Acad Dermatol. 2015;73(1):144-153. doi:10.1016/j.jaad.2015.03.041

Veith AP, Henderson K, Spencer A, Sligar AD, Baker AB. Therapeutic strategies for enhancing angiogenesis in wound healing. Adv Drug Deliv Rev. 2019;146:97-125. doi:10.1016/j.addr.2018.09.010

Vinish, M., Cui, W., Stafford, E., Bae, L., Hawkins, H., Cox, R., and Toliver-Kinsky, T. (2016). Dendritic cells modulate burn wound healing by enhancing early proliferation. Wound Repair Regen 24, 6-13. 10.1111/wrr.12388.

Wolf, F.A., Angerer, P., and Theis, F.J. (2018). SCANPY: large-scale single-cell gene expression data analysis. Genome Biol 19, 15. 10.1186/s13059-017-1382-0.

Wynn TA, Vannella KM. Macrophages in Tissue Repair, Regeneration, and Fibrosis. Immunity. 2016;44(3):450-462. doi:10.1016/j.immuni.2016.02.015

Zhao, J., Patel, J., Kaur, S., Sim, S.L., Wong, H.Y., Styke, C., Hogan, I., Kahler, S., Hamilton, H., Wadlow, R., et al. (2021). Sox9 and Rbpj differentially regulate endothelial to mesenchymal transition and wound scarring in murine endovascular progenitors. Nat Commun 12, 2564. 10.1038/s41467-021-22717-9.